2014

The assimilation of satellite-derived data into a one-dimensional lower trophic level marine ecosystem model

Yongjin Xiao
Virginia Institute of Marine Science

Marjorie A.M. Friedrichs
Virginia Institute of Marine Science, marjy@vims.edu

AGU PUBLICATIONS

JGR

Journal of Geophysical Research: Oceans

RESEARCH ARTICLE

10.1002/2013JC009433

The assimilation of satellite-derived data into a one-dimensional lower trophic level marine ecosystem model

Yongjin Xiao[1] and Marjorie A. M. Friedrichs[1]

[1]Virginia Institute of Marine Science, College of William and Mary, Gloucester Point, Virginia, USA

Key Points:
- Used an ecosystem model in a 1-D data assimilative framework
- Assimilation of satellite-derived size-differentiated chlorophyll and POC
- Assimilating satellite data at multiple sites constrained ecosystem parameters

Correspondence to:
M. A. M. Friedrichs,
marjy@vims.edu

Citation:
Xiao, Y., and M. A. M. Friedrichs (2014), The assimilation of satellite-derived data into a one-dimensional lower trophic level marine ecosystem model, *J. Geophys. Res. Oceans*, *119*, 2691–2712, doi:10.1002/2013JC009433.

Received 12 SEP 2013
Accepted 19 MAR 2014
Accepted article online 24 MAR 2014
Published online 28 APR 2014

Abstract Lower trophic level marine ecosystem models are highly dependent on the parameter values given to key rate processes, however many of these are either unknown or difficult to measure. One solution to this problem is to apply data assimilation techniques that optimize key parameter values, however in many cases in situ ecosystem data are unavailable on the temporal and spatial scales of interest. Although multiple types of satellite-derived data are now available with high temporal and spatial resolution, the relative advantages of assimilating different satellite data types are not well known. Here these issues are examined by implementing a lower trophic level model in a one-dimensional data assimilative (variational adjoint) model testbed. A combination of experiments assimilating synthetic and actual satellite-derived data, including total chlorophyll, size-fractionated chlorophyll and particulate organic carbon (POC), reveal that this is an effective tool for improving simulated surface and subsurface distributions both for assimilated and unassimilated variables. Model-data misfits were lowest when parameters were optimized individually at specific sites; however, this resulted in unrealistic overtuned parameter values that deteriorated model skill at times and depths when data were not available for assimilation, highlighting the importance of assimilating data from multiple sites simultaneously. Finally, when chlorophyll data were assimilated without POC, POC simulations still improved, however the reverse was not true. For this two-phytoplankton size class model, optimal results were obtained when satellite-derived size-differentiated chlorophyll and POC were both assimilated simultaneously.

1. Introduction

Throughout the last two decades, Nutrient-Phytoplankton-Zooplankton-Detritus (NPZD) models have evolved to include more details than those processes in the classic NPZD-type model [*Fasham et al.*, 1990, 1993]. Examples include more sophisticated nutrient limitations [e.g., *Aumont et al.*, 2003; *Cullen et al.*, 2003; *Chai et al.*, 2007; *Dugdale et al.*, 2011; *Mauriac et al.*, 2011], more complex zooplankton grazing [e.g., *Armstrong*, 1999; *Lima et al.*, 2002], nutrient remineralization [e.g., *Moore et al.*, 2002; *Stemmann et al.*, 2004; *Hood et al.*, 2006], and processes associated with dissolved organic nutrients [e.g., *Hood et al.*, 2001; *Druon et al.*, 2010; *Luo et al.*, 2012]. Another common approach for increasing model complexity involves the incorporation of additional phytoplankton and zooplankton compartments [e.g., *Aumont et al.*, 2003; *Le Quere et al.*, 2005; *Fujii et al.*, 2007; *Kishi et al.*, 2007; *Xiao and Friedrichs*, 2014] in order to better represent the reality of the marine ecosystem, which typically includes a myriad of plankton species.

With the increasing number of processes and state variables included in these NPZD-type models, the issue of finding the most appropriate parameter values required by these additional formulations is becoming increasingly critical. Although historically simple NPZD-type models have often been manually calibrated using a trial-and-error method in which parameter values are manually manipulated to attain an improved fit to available data [*Oreskes et al.*, 1994; *Fitzpatrick*, 2009], it is difficult to ascertain whether the resulting calibrated values are truly optimal [e.g., *Rose et al.*, 1991; *Eckhardt and Arnold*, 2001; *Vrugt et al.*, 2003; *Rose et al.*, 2007].

The use of automated methods for identifying optimal parameter values in marine ecosystem models is thus becoming increasingly common. A variety of assimilation methods have achieved a great deal of success in parameter optimization, however one that is very widely used is the variational adjoint method [e.g., *Lawson et al.*, 1995, 1996; *McGillicuddy et al.*, 1998; *Spitz et al.*, 1998; *Fennel et al.*, 2001; *Friedrichs*, 2001; *Leredde et al.*, 2005; *Xu et al.*, 2008, *Luo et al.*, 2010]. Although there have been a few recent exceptions [e.g., *Tjiputra et al.*, 2007; *Fan and Lv*, 2009, *Mattern et al.*, 2012; *Prieß et al.*, 2013], the high computational cost of

implementing these parameter optimization techniques in three-dimensional (3-D) coupled biological-physical ocean models continues to pose a formidable hurdle for many researchers. As a result, modelers often look to first implement such optimization methods with more efficient zero-dimensional or one-dimensional models, before applying the resulting optimal parameters in 3-D. This technique has found considerable success; for example, *McDonald et al*. [2012] demonstrated that parameters optimized in a one-dimensional test bed resulted in significant improvement in the 3-D model framework.

These relatively recent advancements in the field of data assimilative biogeochemical and marine ecosystem modeling have largely been stimulated by the availability of large biological and biogeochemical data sets, particularly satellite products which provide comprehensive synoptic coverage over large regions of the ocean [*Hovis et al*., 1980; *Yoder et al*., 1988; *Hofmann and Friedrichs*, 2001; *McClain*, 2009]. Although chlorophyll concentrations are probably the most commonly used satellite-derived product [e.g., O'*Reilly et al*., 1998; *Carder et al*., 1999; *Yoder et al*., 2002], multiple other satellite-derived products now exist, including: primary production [e.g., *Mouw and Yoder*, 2005; *Marra et al*., 2007], colored dissolved organic matter [e.g., *Hoge and Lyon*, 2002; *Morel and Gentili*, 2009; *Xing et al*., 2012] and particulate organic carbon (e.g., *Mishnov et al*., 2003; *Stramska and Stramski*, 2005; *Stramski et al*., 2008], to name a few. Recent studies have also shown promising progress with regards to deriving phytoplankton size-classes and functional types from satellite ocean color data using "abundance-based approaches" [*Vidussi et al*., 2001; *Uitz et al*., 2006; *Nair et al*., 2008; *Brewin et al*., 2010; *Hirata et al*., 2011] and "spectral-characteristic approaches" [e.g., *Gege*, 1998; *Alvain et al*., 2005; *Pan et al*., 2011]. By definition, these satellite-derived data sets only provide information in the first optical depth, however, this limitation of satellite products is often offset by the large volume of data available both temporally (O(days)) and spatially (O(km)).

As a result of the increasing availability of multiple satellite-derived data sets, there have been a number of studies demonstrating the potential success of assimilating satellite-derived fields for the purposes of both parameter optimization as well as state estimation. State estimation differs from parameter optimization in that the former seeks the best model estimates through reconstructing the system states or more specifically, using statistical procedures to drive the model estimates toward the data [*Gregg et al*., 2009]. Two alternative methods that use satellite data to improve state estimation include the Kalman filter [e.g., *Fontana et al*., 2009; *Hu et al*., 2012; *Mattern et al*., 2010; *Natvik and Evensen*, 2003] and the particle filter [e.g., *Mattern et al*., 2013].

Parameter optimization methods, on the contrary, determine the optimal parameter values that provide a best fit of the model to the data, and as such, result in an improved a posteriori model. Simulations resulting from these methods are required to fit the model equations precisely. These methods, including the variational adjoint technique, have been widely used to parameterize biogeochemical models using satellite data. For example, *Friedrichs* [2002] first demonstrated a 1-D adjoint assimilative framework that minimized model/data misfits using ocean color data from SeaWiFS and illustrated how the assimilative process could help guide model reformulation. *Hemmings et al*. [2004] presented another successful example of assimilating satellite-derived chlorophyll in a depth integrated model, and found the number and geographic scope of particular parameter sets that generated the best fit to validation data. With the significant advances in computational power over the past decade, there have also been a handful of studies assimilating satellite-derived chlorophyll data into 3-D models (e.g., *Garcia-Gorriz et al*., 2003; *Tjiputra et al*., 2007; *Fan and Lv*, 2009]. In all of these examples, however, only total chlorophyll was assimilated; other types of satellite-derived data such as POC and size differentiated chlorophyll were not assimilated.

In contrast to these previous satellite data assimilation efforts, in this study satellite-derived POC and size-differentiated chlorophyll are assimilated in addition to total chlorophyll. To better understand whether the assimilation of these multiple types of satellite data can constrain a one-dimensional (vertical) lower tropic level model, an existing data assimilative framework was implemented in this study at four sites in the Mid-Atlantic Bight (Figure 1). Experiments assimilating synthetic data (i.e., numerical twin experiments) as well as experiments assimilating actual satellite-derived fields (total chlorophyll, size-differentiated chlorophyll, and POC) were conducted in order to assess the ability of the assimilation framework to optimize key biogeochemical parameters, and to assess which types of satellite-derived data may best constrain the model. The following section describes in detail our lower trophic level model, the assimilative framework, the satellite-derived data to be assimilated, and the assimilation experiments. Section 3 presents the results

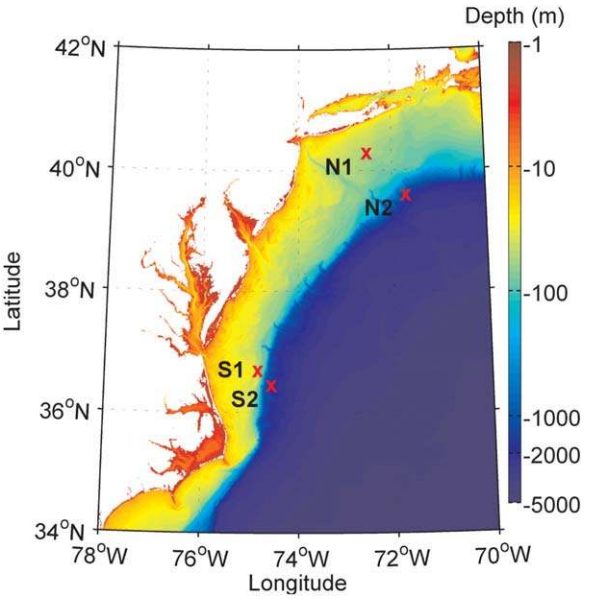

Figure 1. Locations of the four study sites.

from the assimilation experiments while section 4 discusses the implications of these results. Lastly, a summary is provided in section 5.

2. Methods

2.1. One-Dimensional Model

2.1.1. Lower Trophic Level Model

The lower trophic level model used here (Figure 2, Appendix A) is a nitrogen-based Fasham-type [*Fasham et al*., 1990, 1993] model with nine state variables: large and small phytoplankton, large and small chlorophyll, large and small detritus, zooplankton, ammonium, and nitrate. The chlorophyll to carbon ratios of the phytoplankton are variable, and nonlinear due to the effects of photoacclimation [*Geider et al*., 1997]. The model is similar to that described by *Fennel et al*. [2006], which was originally developed for the Mid-Atlantic Bight (MAB), but which has subsequently been successfully applied to a number of other shelf systems [e.g., *Fennel et al*., 2011; *Gan et al*., 2010; *Hofmann et al*., 2008, 2011; *Xue et al*., 2013] The modifications made to the original *Fennel et al*. [2006] version of this model are described below.

The single phytoplankton and chlorophyll compartments in the original model were broken down into two size classes, representing picophytoplankton plus nanophytoplankton and microphytoplankton. This was motivated by the fact that this region is characterized by two distinct phytoplankton size classes, with the larger microphytoplankton contribution to total chlorophyll being large on the inner MAB shelf ($>$ 30%) and small in off-shelf waters [*Mouw and Yoder*, 2005]. The inclusion of a second phytoplankton size class in the model requires two additional equations (for size-specific phytoplankton and chlorophyll; see Appendix A) and the specification of six new parameters for the second phytoplankton size class (Table 1). Remaining biological parameters, processes and formulations, including sediment denitrification, were identical to those listed in *Fennel et al*. [2008]. (Note that the parameters in *Fennel et al*. [2008] include some variants on the original values provided in *Fennel et al*. [2006]. Here the modified parameters listed in *Fennel et al*. [2008] have been adopted.) Model estimates of POC were computed as the sum of the small and large phytoplankton, small and large detritus, and zooplankton, and then converted from nitrogen to carbon units using the Redfield ratio of C:N = 6.625 moleC/moleN.

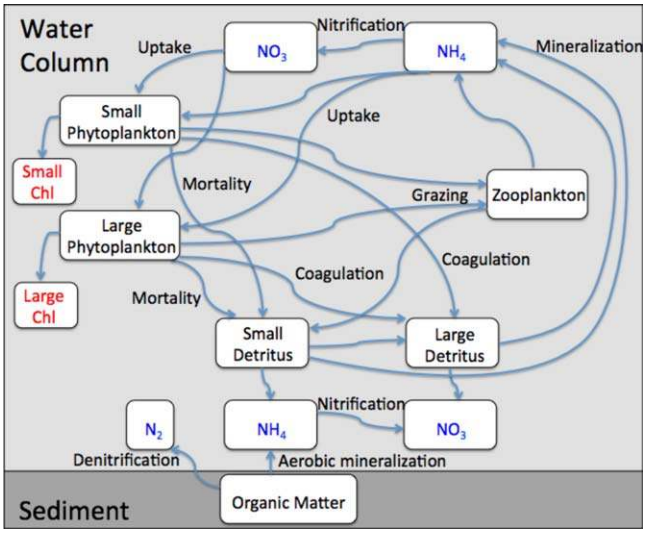

Figure 2. Schematic diagram showing linkages between the various state variables in the 2P1Z ecosystem model.

Table 1. New Ecosystem Model Parameters That Are Required for the 2P1Z Model Used in This Study[a]

Parameter	Unit	Small Phytoplankton	Large Phytoplankton
Maximum chlorophyll to carbon ratio	mgChl mgC^{-1}	0.03	0.06
Phytoplankton growth rate at 0°C	d^{-1}	1.8	1.0
Sinking rate of phytoplankton	$m\ d^{-1}$	0.1	0.4
Half-saturation concentration for uptake of NH_4	$mmol\ N\ m^{-3}$	0.5	1.0
Half-saturation concentration for uptake of NO_3	$mmol\ N\ m^{-3}$	1.0	1.5
Maximum grazing rate	$(mmol\ N\ m^{-3})^{-1}\ d^{-1}$	0.8	1.2

[a]All remaining ecosystem parameters are identical to those used by *Fennel et al*. [2008] for their 1P1Z model.

Following *Friedrichs et al*. [2007], the differential equations in the biological model were solved using a second-order Runge-Kutta scheme.

2.1.2. Physical Model

The lower trophic level model described above was embedded into the 1-D (vertical) physical model used by *Friedrichs et al*. [2006, 2007]. The model was forced by time series of solar radiation, temperature, vertical diffusivity, vertical velocity, and mixed-layer depth. Photosynthetically active radiation was calculated as a fraction (0.43) [*Pinker et al*., 2010] of the shortwave radiation flux obtained from the North American Regional Reanalysis generated by the National Center for Environmental Prediction. The remaining fields were acquired from a 3-D coupled biogeochemical-circulation model simulation generated by the Regional Ocean Modeling System (ROMS) [*Shchepetkin and McWilliams*, 2005] and configured for the Northeast North American shelf using the original single phytoplankton *Fennel et al*. [2006] model configuration (NENA) [*Hofmann et al*., 2008, 2011].

Vertical advection and particle sinking processes were computed using a third-order direct space-time upwind-biased scheme [*Hundsdorfer and Trompert*, 1994] with the Sweby flux limiter [*Sweby*, 1984]. Following *Friedrichs et al*. [2006, 2007], vertical diffusion was solved by applying a Crank-Nicholson vertically variable diffusion operation and all state variables were redistributed homogeneously within the mixed layer at the end of each time step.

2.1.3. Forward Model Implementation

Initial and bottom boundary conditions for the model state variables were provided by the 3-D NENA model. Initial conditions were directly obtained from the first 3 day averaged NENA output in year 2004 except for the size-fractionated phytoplankton and associated chlorophyll. The model is not sensitive to the initial size-fractionated ratio and thus the two size-classes of phytoplankton and chlorophyll were each initialized as one half the NENA concentrations. Boundary conditions were likewise obtained from the 3 day averaged NENA output. For sites shallower than 200 m, the bottommost layer was used; for sites deeper than 200 m, the bottommost layer in the 1-D model was set to 200 m and the boundary condition was obtained from the corresponding depth.

The model was run from 1 January 2004 through 31 December 2004 with a time step of 1 h at four sites within the MAB (Figure 1). Two sites (N1 and S1) were located on the shelf (depth ~50 m and ~100 m) and two sites (N2 and S2) were located near the shelf break (depth ~800 m and ~600 m). Vertical resolution varied according to bottom depth, but was higher nearer the surface (~0.3 to 2 m) and larger at depth (~3 to 8 m).

2.2. Variational Adjoint Method

The variational adjoint method [e.g., *Lawson et al*., 1995] was used to objectively minimize model-data misfits by optimizing the biological parameters. The cost function, J, represents the misfit between each model estimate (a) and the corresponding observation ($\hat{a}$) and is computed as a weighted sum of squared differences between the model and the data:

$$J=\frac{1}{M}\sum_{k=1}^{K}\sum_{m=1}^{M}\frac{1}{N_{km}\cdot\sigma_{km}^{2}}\sum_{j=1}^{N_{km}}\left(a_{jkm}-\hat{a}_{jkm}\right)^{2} \quad (1)$$

where K is the number of sites, M is the number of data types, N_{km} is the number of observations for each data type and site, and σ_{km} is the standard deviation of these data (see Table 2). In this way, the cost

Table 2. Number of Observations (N), Mean and Standard Deviation (σ_{km}) of the Satellite-Derived Chlorophyll Concentrations (mgChl m^{-3}) and POC Data (mgC m^{-3}) at Each Site

	Small-Size Chl			Large-Size Chl			POC		
	N	Mean	σ_{km}	N	Mean	σ_{km}	N	Mean	σ_{km}
N1	108	0.41	0.30	108	0.22	0.22	119	134	48
N2	90	0.31	0.36	90	0.16	0.31	94	112	78
S1	122	0.44	0.33	122	0.24	0.25	124	140	54
S2	121	0.33	0.26	121	0.16	0.17	124	109	48

function provides an estimate of the ratio between the model-data differences and the differences between the data and the mean of the data, i.e., σ_{km}^2. Thus, the cost function equals one at each site when the sum of the squared model-data differences equals the variance of the data [*Friedrichs et al*., 2007]. Furthermore, two cost functions are considered to be insignificantly different if their difference is less than one for a single site, or less than the number of sites when multiple sites are included in the calculation.

The variational adjoint method requires: (i) adjoint code used to compute the gradient of the cost function with respect to the control parameters, defined as the subset of model parameters to be optimized, and (ii) an optimization procedure used to search for the optimal values of these control parameters that generate the smallest possible cost function. In this study, the adjoint code was obtained from the Tangent linear and Adjoint Model Compiler (TAMC) [*Giering and Kaminski*, 1998]. Parameter optimization is performed by a limited memory quasi-Newton optimization procedure [*Gilbert and Lemaréchal*, 1989].

After the cost function is computed from an a priori forward model run, the adjoint code computes the gradients of the cost function and passes the information to the optimization procedure, which determines how much each control variable should be modified in order to reduce the magnitude of the cost function. The new values of the control parameters are then used in the forward model, the new cost function is computed, and the optimization procedure is repeated. These iterations continue until the specified convergence criterion is satisfied.

Control variables were selected based on two considerations: (1) the sensitivity of the cost function to the parameter values and (2) the correlations between parameters. The sensitivity of the cost function to each model parameter was estimated by computing $(J_{sens} - J_{ref})/J_{ref}$, where J_{ref} is the cost function using the reference parameters and J_{sens} assumes a +25% or −25% change in each individual model parameter [*Friedrichs and Hofmann*, 2001; *Friedrichs*, 2001]. The results of this sensitivity analysis (Table 3) indicated that the model is most sensitive to parameters in the phytoplankton equations, with only one exception, i.e., the zooplankton basal metabolism rate.

Previous studies have demonstrated that strongly correlated parameters cannot be simultaneously optimized, since in this case the model would be able to generate multiple optimal values for the control variables [e.g., *Matear*, 1995]. Following the sensitivity analysis, assimilation experiments were conducted to investigate the correlations of all parameters with sensitivities greater than 5% (Table 3) using the inverse of the Hessian matrix [*Thacker*, 1989; *Matear*, 1995; *Friedrichs*, 2002]. The five parameters ultimately selected as control variables based on their relatively low correlations were the maximum Chl:C ratios for the large and small phytoplankton, the maximum growth rates for the large and small phytoplankton, and the zooplankton basal metabolism rate.

Table 3. Parameter Sensitivities Computed as a Percent Change in the Cost Function Resulting from +25% and −25% Changes in Parameter Values[a]

Parameter	+25% Sensitivity	−25% Sensitivity	Absolute Mean Sensitivity
Maximum chlorophyll to carbon ratio	26%	−16%	21%
Half-saturation concentration for uptake of NO_3	7%	−4%	6%
Half-saturation concentration of phytoplankton ingestion	9%	−8%	9%
Phytoplankton growth rate at 0°C	9%	−7%	8%
Zooplankton basal metabolism rate	8%	−4%	6%

[a]Results are shown for all parameters with absolute mean sensitivities greater than 5%.

2.3. Satellite-Derived Data

Three types of data were derived from the Sea-viewing Wide Field-of-view Sensor (SeaWiFS) and assimilated into the lower trophic level model: total chlorophyll *a* (Tot_Chl), size-fractionated chlorophyll *a* divided into large chlorophyll (ChlL) and small chlorophyll (ChlS), and POC. Although depth-integrated productivity estimates are also routinely computed from satellite-derived fields using ocean color productivity models, the uncertainties associated with the resulting fields can be as large or larger than estimates derived from biogeochemical ocean circulation models [*Friedrichs et al*., 2009] and one-dimensional ecosystem models [*Saba et al*., 2011]. As a result, these productivity fields were not selected for assimilation.

Size-fractionated chlorophyll was determined through a three-step process. First, phytoplankton pigment concentrations were computed using an algorithm specifically proposed for the MAB continental shelf [*Pan et al*., 2010]. The phytoplankton pigments were then analyzed by CHEMTAX (a chemotaxonomic analysis) to quantify 11 taxonomic groups based on pigment distributions [*Pan et al*., 2011]. Lastly the resulting 11 taxonomic groups were categorized into three size-classes based on *Vidussi et al*. [2011]: picophytoplankton, nanophytoplankton, and microphytoplankton. Since the model in this study only includes two size classes, the nanophytoplankton was combined with the picophytoplankton data to represent the small size class. This decision was based on the distinction between microphytoplankton and smaller phytoplankton in terms of sinking rates, surface-to-volume ratios, and recycling rates [*Lomas and Moran*, 2011]. Tot_Chl concentrations were computed by summing the two size-classes of chlorophyll described above. The resulting chlorophyll concentrations agreed well with chlorophyll obtained from the standard OC4v4 algorithm [*O'Reilly et al*., 2000], with the average absolute difference being less than 0.3 mg Chl m^{-3}. Surface POC was computed using an empirical algorithm based on the ratio of bandwidths at 490 and 555 nm [*Stramska and Stramski*, 2005]. Although these satellite data were all derived using empirical or semianalytical algorithms, they have demonstrated considerable success in their agreement with in situ data. The uncertainty associated with these size-differentiated chlorophyll and POC concentrations have been estimated to be 35% [*Pan et al*., 2010; *Stramska and Stramski*, 2005].

2.4. Assimilation Experiments

2.4.1. Identical Twin Assimilation Experiments

The assimilation of model-generated synthetic data in numerical twin experiments provides a useful tool for demonstrating the feasibility of an assimilation method [e.g., *Lawson et al*., 1996; *Crispi et al*., 2006; *Hemmings and Challenor*, 2012; *Pelc et al*., 2012], investigating the adequacy of available observations [e.g., *Spitz et al*., 1998; *Friedrichs*, 2001], as well as determining sensitivities and correlations of the optimized parameter sets [e.g., *Schartau et al*., 2001; *Fennel et al*., 2001; *Kuroda and Kishi*, 2004; *Kidston et al*., 2011].

In this study, as an initial test of the variational adjoint assimilation framework twin experiments were conducted in which synthetic chlorophyll and POC data generated by the model were assimilated. The twin experiment methodology includes two simulations. The first is the "true simulation" generated using the a priori, or "true parameter" values. The synthetic data are obtained by subsampling the "true simulation" at the times when actual satellite data are available. These synthetic data are then assimilated into a second model run, the "initial simulation," which uses randomly generated initial estimates of the control parameters (in this case using a range of $\pm 25\%$ of the original values). Ideally, the assimilation procedure should be able to recover the "true" values of the control parameters used to generate the synthetic data, and therefore also reproduce the "true simulation" perfectly.

Two different types of twin experiments were conducted. In the "Individual Assimilation" experiments, synthetic data were assimilated at each of the four sites (Figure 1) individually, resulting in four sets of optimal parameters (one set for each site). The costs were then summed in order to obtain a single cost value for the Individual Assimilation experiment. In the second "Simultaneous Assimilation" experiment, the synthetic data were simultaneously assimilated from all four sites, resulting in one best fit set of optimal parameters for all four sites. For each type of experiment, five different cases were examined, in which different data types were assimilated: (1) ChlL+ChlS+POC, (2) Tot_Chl+POC, (3) ChlL+ChlS, (4) Tot_Chl, and (5) POC.

In reality, ocean data are never perfect, and instead are inevitably associated with measurement errors or uncertainties, which will reduce the ability of an optimization procedure to recover actual ecological rate parameters for a given system. Thus, in addition to assimilating the "perfect" synthetic data set as described in the identical twin experiments above, additional numerical twin experiments were conducted for Case 1

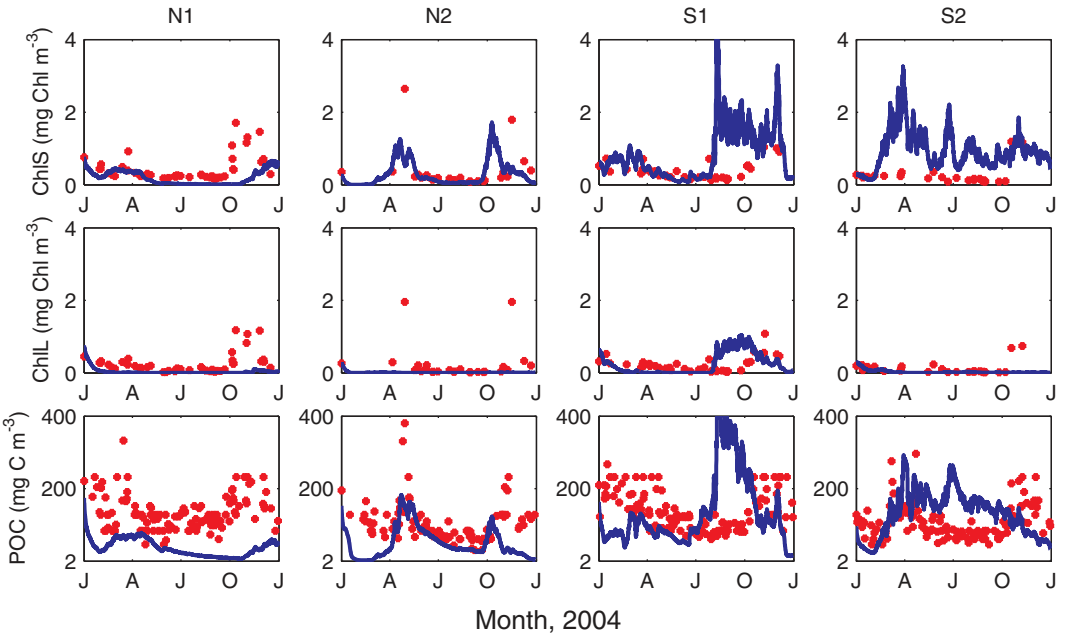

Figure 3. (top and middle rows) Time series of size-differentiated surface chlorophyll and (bottom row) surface POC from the satellite-derived data (red closed circles) and the a priori simulation (blue lines) at the four study sites.

(assimilating ChlL+ChlS+POC) in which the assimilated synthetic data included five different levels of normally distributed random noise (2.5%, 5%, 10%, 20%, and 40%).

2.4.2. Satellite Assimilation Experiments

In a final series of experiments, actual satellite-derived data fields were assimilated in both Individual and Simultaneous Assimilation experiments. As described above, each of these two types of experiments again involved five cases to assess the effects of assimilating different data types: (1) ChlL+ChlS+POC, (2) Tot_Chl+POC, (3) ChlL+ChlS, (4) Tot_Chl, and (5) POC. In these experiments, two different costs are computed. First, the "Assimilation Cost" is reported as the final a posteriori cost for the specific data that were assimilated. Secondly, the "Total Cost" is computed using equation (1) for ChlL+ChlS+POC for each case, independent of which of these data types were assimilated. The latter Total Cost is used as a common metric to compare the relative performance of the five cases. According to these definitions, the Assimilation Cost and the Total Cost are identical in Case 1.

3. Results

3.1. A Priori Model-Data Comparison

The a priori simulation produced surface estimates of chlorophyll and POC that were generally within the same range as the satellite-derived data (0–3 mgChl m^{-3} and 0–200 mgC m^{-3}, respectively, Figure 3). In general, the data indicated similar concentrations for the ChlL and ChlS, whereas the model generally showed higher ChlS concentrations. The timing of the blooms was generally not particularly well represented in the model estimates, except for the spring bloom of ChlS at the N2 site, which was accurately captured in the model. As was the case for chlorophyll, the model underestimated POC at the northern sites, although the temporal trends of the data (spring and fall peaks) were moderately well resolved. At the southern sites, the POC model estimates were again comparable to the data in terms of magnitude, but out of phase in time. Specifically, the simulated POC and chlorophyll were in phase, whereas the satellite-derived POC and satellite-derived chlorophyll were not.

Simulated vertical distributions of chlorophyll and POC demonstrated pronounced subsurface maxima only at the southern onshore site (Figure 4) resulting from strong nutrient upwelling, which contributed to significant ChlL concentrations [*Ryan et al.*, 1999]. Somewhat weaker subsurface maxima were also present at the offshore northern site, but were absent at the other two sites (N1 and S2) where the water column was

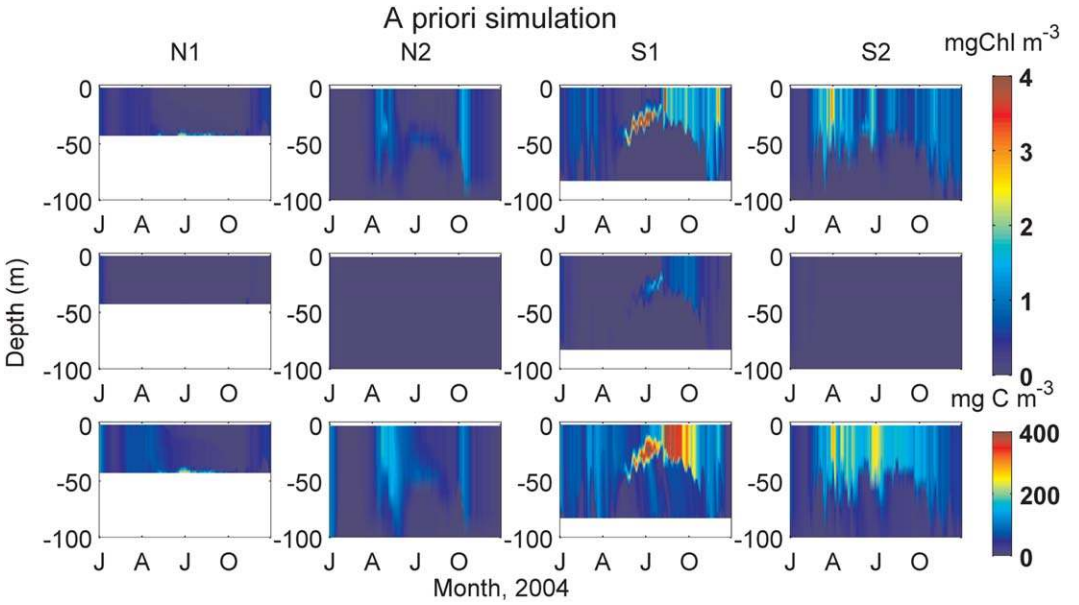

Figure 4. Depth-time plots of size-differentiated chlorophyll (top row: ChlS; middle row: ChlL) and (bottom row) POC from a priori simulation at the four study sites.

typically well mixed down to at least 40 m. Overall, lower chlorophyll concentrations were found at the northern sites where phytoplankton were more consistently nutrient limited. Despite the fact that detritus accounted for a substantial portion of particulates, simulated POC covaried closely with chlorophyll within the euphotic zone.

The total cost for the a priori simulation summed over the four sites was 15 (Figure 5). The model-data misfit for small phytoplankton was the largest component of the total a priori cost, which was primarily caused by the overestimates of ChlS at the two southern sites (Figure 3). In contrast, the large phytoplankton component was consistently underestimated by the model, resulting in relatively low ChlL costs (Figure 5). The cost resulting from POC model-data misfits was slightly smaller than the ChlS contribution, but was similarly dominated by misfits at the southern sites.

3.2. Twin Experiments

Assimilation of synthetic data with the same sampling frequency as the satellite data enabled an exact recovery of the initial "true" values of all five control parameters in both the Individual and the Simultaneous Assimilation experiments, with costs reaching 10^{-10} after only 15–25 iterations (Table 4, Figure 6). This was true not only for Case 1 (assimilating ChlL+ChlS+POC; Figure 6) but also for the other four cases assimilating different combinations of satellite-derived data (not shown). Four additional Simultaneous Assimilation experiments were conducted in which only a portion of the synthetic data points for the ChlL+ChlS+POC case was assimilated (one half, one quarter, one eighth, and one sixteenth), and all four experiments again resulted in perfect parameter recoveries.

When random noise was added to the synthetic data prior to assimilation, the initial "true" values of the five control parameters were no longer recovered perfectly. As the level of noise increased in the data, the optimized parameter values increasingly deviated from the initial "true" parameters. This deviation was significantly greater when the noisy synthetic data were assimilated individually at each site (Figure 6a), as compared to the values optimized by assimilating data simultaneously at all four sites (Figure 6b). For the Individual Assimilation experiment, the maximum parameter deviation was more than 1000% for the run with 40% noise, whereas the Simultaneous Assimilation experiment resulted in maximum parameter deviations of less than 10% (Figure 6).

Because the addition of noise to the synthetic data prevented the true parameter values from being recovered exactly, the a posteriori cost functions were significantly larger in the presence of noise (Table 4). In contrast to the very different results seen for the values of the optimized parameter values in the two

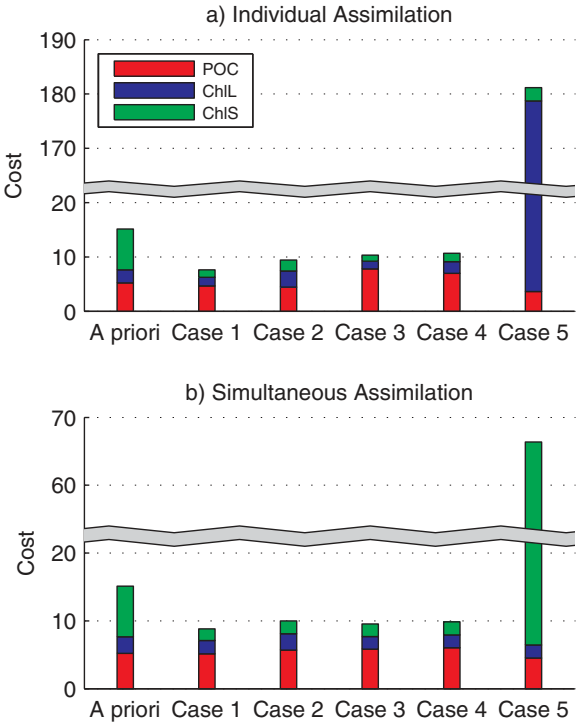

Figure 5. Total cost functions (ChlS+ChlL+POC) resulting from (a) the Individual Assimilation and (b) the Simultaneous Assimilation experiments in which five different types of data (Cases 1–5) were assimilated.

experiments (Figure 6) the a posteriori cost values were quite similar for both the Individual and Simultaneous Assimilation experiments (Table 4): for both experiments costs ranged from $\sim 10^{-3}$ (2.5% noise) to 0.3 (40% noise). In both experiments, the a posteriori costs were lower than the costs computed for the misfit between the true simulation and the assimilated noisy data ("true cost"; Table 4), indicating that the parameter values generated by the optimization process ultimately fit the noisy synthetic data better than did the original "true" parameters that were used to generate the noisy data.

3.3. Assimilation of Satellite-Derived Data: Individual Assimilation Experiments

When the actual satellite-derived size-differentiated chlorophyll and POC concentrations were assimilated (Case 1) at individual sites, the Total Cost was reduced by nearly half (Table 5). Although slight cost reductions occurred for all three cost components (Figure 5a), the cost component corresponding to ChlS was responsible for more than 80% of the overall reduction in the cost function. Improvements in the model-data misfit were also evident from the time series of ChlL, ChlS, and POC: the a posteriori time series of all three components (ChlS, ChlL, and POC; Figure 7a) fit the satellite data better than the a priori time series (Figure 3). In addition, the assimilation procedure also affected the subsurface distributions, particularly at sites N2, S1, and S2 (Figure 8a). Throughout the water column, the ChlS fields generally decreased after assimilation (except at the N2 site during the spring bloom), whereas ChlL generally increased (except at the S1 site during the fall bloom). The POC anomalies showed more pronounced variability, both temporally (e.g., at the N2 site, where increases were only found in the summer) and spatially (e.g., at the S1 and S2 sites, where increases were primarily found at depth; Figure 8a).

In order to identify the relative importance of assimilating different types of satellite-derived data, four other assimilations cases, i.e., assimilating Tot_Chl+POC, ChlL+ChlS, Tot_Chl, and POC, were also performed. Significant reductions in the Individual Assimilation Costs were generated with all assimilation cases (Table 5). However, a more robust test of the assimilation procedure involves examining whether improvements in model skill are also generated for data that are not assimilated [*Gregg et al.*, 2009]. To assess the degree of improvement for the nonassimilated variables as well as to more equitably compare the relative performance of the five assimilation cases, the cost functions corresponding to ChlL, ChlS, and POC, i.e., the Total Costs, were computed for all five cases (Figure 5a, Table 5). As expected, the smallest Total Cost was generated by Case 1, which

Table 4. Case 1 Cost Functions for Twin Experiments Assimilating Noisy Synthetic Data

Max. Noise (%)	A Priori Cost	Individual Cost	Simultaneous Cost	"True" Cost[a]
0	0.367	$<10^{-10}$	$<10^{-10}$	$<10^{-10}$
2.5	0.376	0.001	0.001	0.001
5	0.366	0.003	0.004	0.004
10	0.367	0.015	0.016	0.017
20	0.364	0.052	0.056	0.060
40	0.711	0.275	0.297	0.308

[a]"True" cost represents the cost corresponding to the true simulation and the noisy synthetic data.

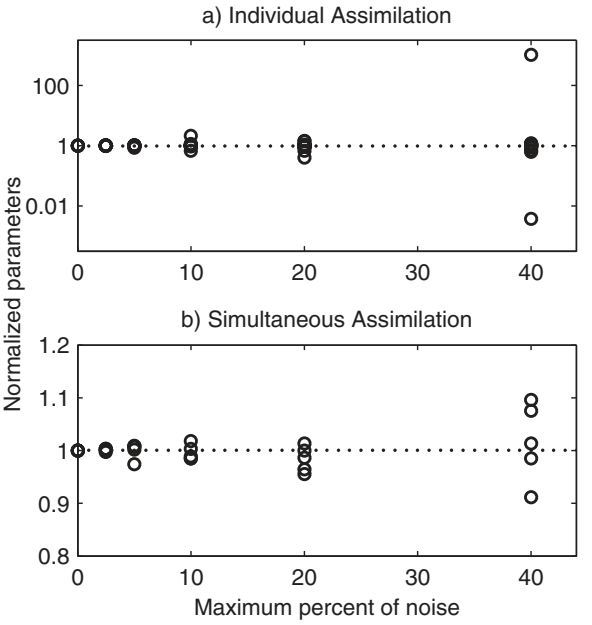

Figure 6. Optimized parameter values normalized to the true values from the twin experiments with varying levels of noise added to the synthetic data after (a) the Individual Assimilation and (b) the Simultaneous Assimilation. Note differences in *y* axis scales.

specifically assimilated these three variables. However, when total chlorophyll was assimilated but the size-fractionated information was not (i.e., Cases 2 and 4), significant improvements in the relative abundance of ChlS were still produced (Figure 5a). When POC data were not assimilated (Cases 3 and 4), the model-data fit for POC deteriorated only very slightly; in contrast, when chlorophyll data were not assimilated (Case 5), the cost functions associated with the unassimilated size-fractionated chlorophyll (ChlL) increased by a factor of 12 (Figure 5a).

Although these Individual Assimilation experiments reduced the Assimilation costs for all five cases (Table 5), an examination of the optimized parameter values (Figure 9a) revealed that in each case this was accomplished by means of optimized parameter values that were adjusted by multiple orders of magnitude. As will be discussed more extensively in section 4, this is indicative of an overtuned model simulation: the model is capable of fitting the assimilated data relatively well in every case, but in each instance it does so through the use of highly unrealistic parameter estimates.

3.4. Assimilation of Satellite-Derived Data: Simultaneous Assimilation Experiments

The assimilation of ChlL+ChlS+POC data from all four sites simultaneously (Case 1) resulted in only a slightly larger cost (8.8) than that obtained by optimizing the model for all four sites individually (7.6; Table 5). When decomposing the Total Cost into the three components (ChlL+ChlS+POC), the Simultaneous Assimilation experiments again resembled the Individual Assimilation experiments (Figure 5b) in that ChlS accounted for the majority of the reduction in the cost function (>90%). This assimilation also again led to substantial changes in the vertical distributions of the assimilated state variables. In fact, the largest anomalies (a posteriori simulation minus a priori simulation) in the three variables were often found in subsurface layers, e.g., deep POC increased dramatically at the S1 site after assimilation (Figure 8b). Overall, these results illustrate that assimilating surface data alone can generate far-reaching effects in the subsurface distributions.

As expected, for all five cases simultaneously assimilating various combinations of satellite-derived data, the reduction in the Assimilated Costs was smaller than those derived from the Individual Assimilation experiments (Table 5). However, the five cases resembled the Individual Assimilation experiments in relative performance, i.e., the cases without the assimilation of POC (Cases 3 and 4) resulted in the lowest Assimilated Costs.

Table 5. Assimilation Costs and Total Costs for Experiments Assimilating Actual Satellite Data in the Individual and Simultaneous Experiments

Case	Assimilated Variables	A Priori Assim. Cost	Individ. Assim. Cost	Individ. Total Cost	Simul. Assim Cost	Simul. Total Cost
1	ChlS+ChlL+POC	15.1	7.6	7.6	8.8	8.8
2	Tot_Chl+POC	9.3	6.0	9.4	7.5	10.0
3	ChlS+ChlL	9.9	2.5	10.3	3.7	9.5
4	Tot_Chl	4.1	1.3	10.7	1.8	9.9
5	POC	5.2	3.7	181	4.5	66

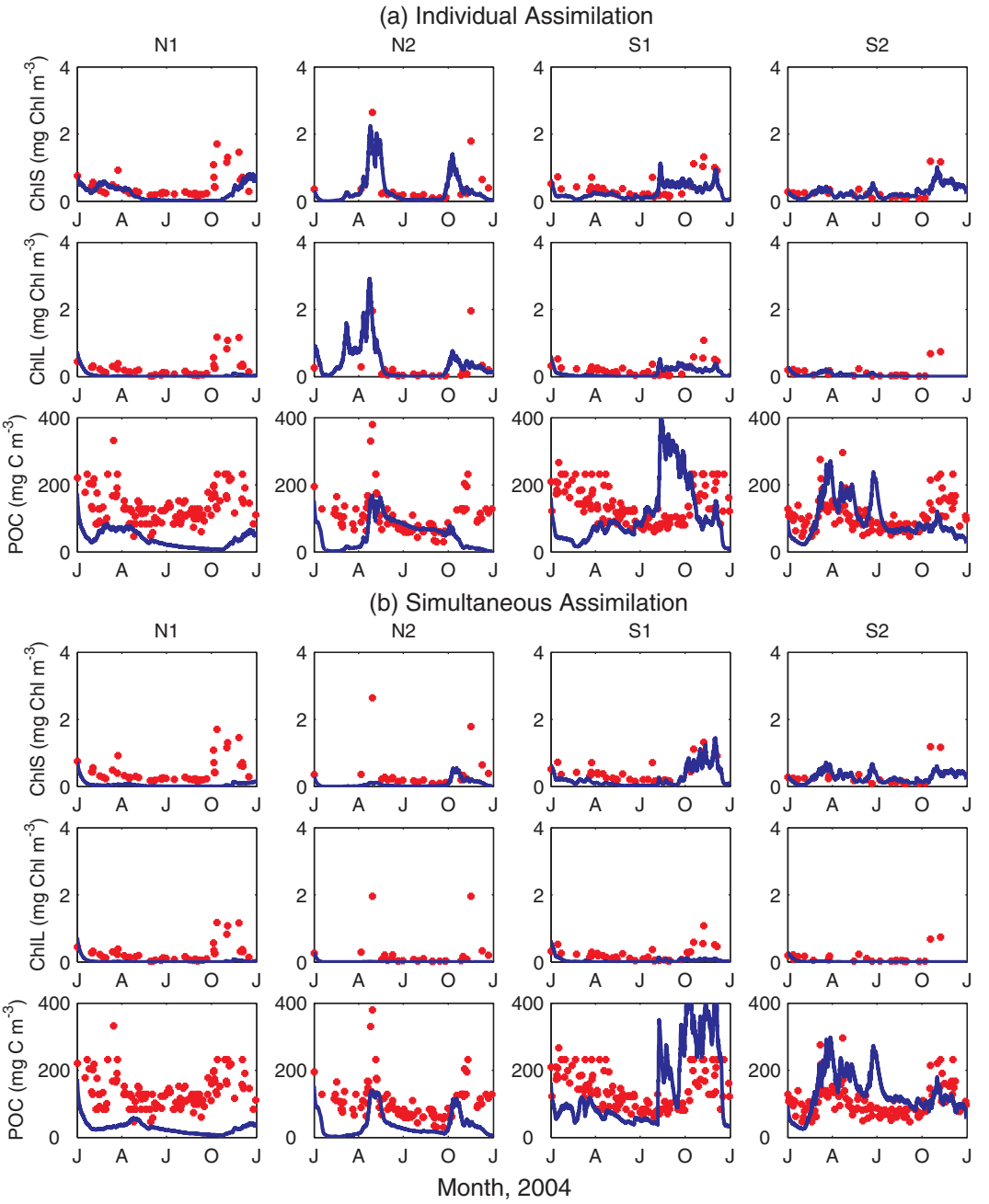

Figure 7. Time series of size-differentiated surface chlorophyll and surface POC for the satellite data (red closed circles) and the simulations (blue lines) at all four study sites after (a) the Individual Assimilation and (b) the Simultaneous Assimilation.

In terms of Total Costs, the results of the Simultaneous Assimilation experiments were again consistent with those obtained from the Individual Assimilation experiments (Figure 5). Specifically, Total Cost increased when POC was assimilated without chlorophyll (Case 5), whereas Case 1 produced the lowest Total Cost. Results from Cases 2 and 4 were very similar to each other suggesting that when total chlorophyll data were assimilated, the additional assimilation of POC data did not result in significant further improvement. While the assimilation of POC alone (Case 5) resulted in high ChlL model-data misfits for the Individual experiments, this resulted in high ChlS model-data misfits for the Simultaneous experiments. Overall, these results indicated that the model was able to constrain the POC field even when chlorophyll data were assimilated without POC data; however, the model was not able to constrain the chlorophyll field when assimilating POC data without chlorophyll data (see section 4.3).

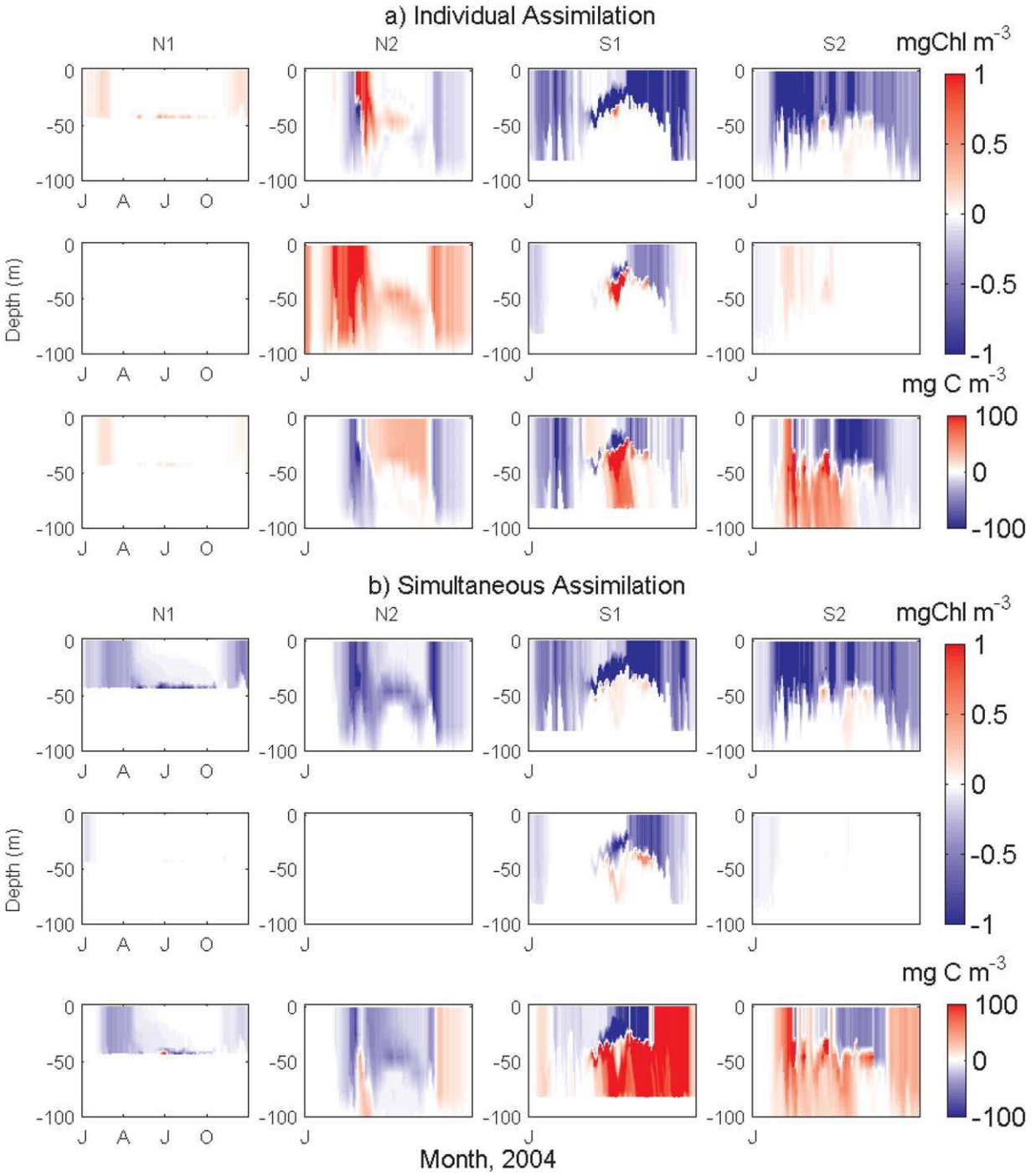

Figure 8. Anomalies (a posteriori simulation—a priori simulation at the four study sites for (a) the Individual Assimilation and (b) the Simultaneous Assimilation, in each experiment for (top rows) ChlS, (middle rows) ChlL, and (bottom rows) POC.

Although the Simultaneous Assimilation experiments always produced higher Assimilation Costs than the Individual Assimilation experiments (Table 5), they generated lower Total costs in Cases 3, 4, and 5 (Table 5, Figure 5b). In these particular cases for which only a single type of data (size-differentiated chlorophyll, total chlorophyll, or POC) was assimilated, the Individual Assimilation experiments did not provide enough information to successfully constrain the model. As a result, the model overtuned the parameters to adequately fit the assimilated variable, but at significant cost to the model-data misfit for the other unassimilated

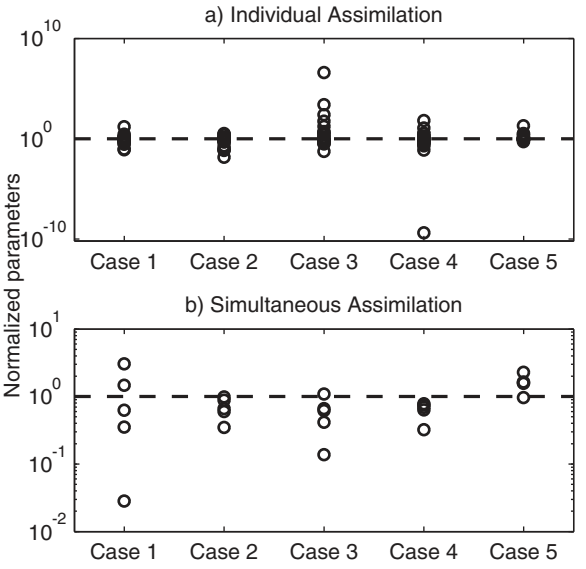

Figure 9. Optimized parameter values normalized to the initial guesses after (a) the Individual Assimilation and (b) the Simultaneous Assimilation of actual satellite data in which five different types of data (Cases 1–5) were assimilated. Note differences in *y* axis scales.

variables. In contrast, when a single type of data was assimilated at all four sites simultaneously, the model was better constrained and as a result the costs for the unassimilated variables were lower than they were when the data were assimilated at each site individually (Figure 5).

The greatest difference between the Simultaneous and Individual experiment results were the optimal parameter values obtained from the assimilation procedure (Figure 9b). The five Simultaneous Assimilation cases produced optimized parameter values that were all within a reasonable range (10^{-2}–10^{2} times original values), whereas the Individual Assimilation cases produced multiple parameter values that were many orders of magnitude different from the original values.

4. Discussion

4.1. Simultaneous Assimilation of Noisy Synthetic Data: Quantification of Success

The success of an optimization experiment is a function not only of how well a model represents the key biological and physical processes inherently characterizing the assimilated data, but also the specific parameters chosen for optimization and the quality/quantity of the data assimilated. Numerical twin experiments are a useful technique for assessing potential problems that may arise from either of the latter two issues. By examining both the true versus optimized parameter values and the true versus optimized simulated distributions, it is possible to assess the potential success of an assimilation framework. Here the success of optimizing a 1-D model by assimilating 1 year of satellite data (including size-differentiated chlorophyll, total chlorophyll, and/or POC) has been tested under conditions of varying levels of random noise.

The presence of 40% noise in the assimilated synthetic satellite data resulted in the optimized parameters deviating from the true parameter values by less than 10%, indicating that relatively successful parameter recoveries are possible even in the presence of significant noise in the assimilated satellite data. These results are consistent with those found in previous studies. For example, *Lawson et al.* [1995] and *Kidston et al.* [2011] both demonstrated that in the presence of 20% noise, the optimized parameters were only slightly different from the true parameters when surface data were assimilated every few days. *Friedrichs* [2001] also showed that model skill was significantly improved even when assimilating synthetic data associated with 40% noise, especially when long time series of data were available for assimilation, as is typically the case for satellite data.

Although the success of twin experiments are generally quantified by how well the true control parameters are recovered [*Lawson et al.*, 1995; *Kidston et al.*, 2011; *Friedrichs*, 2001; *Spitz et al.*, 1998; *Pelc et al.*, 2012], another important test of the success of the assimilation process involves determining how well the optimized simulation reproduces the true simulation. This is a considerably more robust test of the assimilation process as it involves examining whether the assimilation improves unassimilated distributions [*Gregg et al.*, 2009]. Here the optimized and true simulations were compared for the experiment assimilating Case 1 synthetic data with 40% noise by means of root-mean squared differences (RMSD) [*Stow et al.*, 2009]. The RMSD computed between the simultaneously optimized simulation and the true simulation (Table 6) was 77%–85% smaller than that computed between the initial simulation and the true simulation, not only for the assimilated data types (i.e., chlorophyll and POC), but also for unassimilated variables (i.e., nitrate and primary productivity).

Table 6. Root-Mean Squared Differences (RMSD) for the Twin Experiments, Before and After Optimization[a]

	Data Type	Initial Model RMSD	Individ. Optimization RMSD	Simul. Optimization RMSD
Surface layer	Chl	0.5	0.2	0.1
	POC	48.3	15.1	7.4
	NO_3	0.7	0.3	0.1
	PrPr	52.0	23.0	11.4
Sum of upper 15 layers	Chl	6.2	2.3	1.3
	POC	629	207	99
	NO_3	9.7	3.7	1.7
	PrPr	416	188	83

[a]All RMSD were computed between the true simulation and (1) the model before assimilation (representing the initial model error), (2) the 40% noisy data (representing the data error), and (3) the optimized model (representing the assimilation error) for distributions of Chlorophyll (Chl; mgChl m^{-3}), POC (mgC m^{-3}), nitrate (NO_3; mmol N m^{-3}), and primary production (PrPr; mgC m^{-3} day^{-1}).

Another method for assessing the success of assimilation experiments involves examining whether model-data fit improves at depths where data were not assimilated. In this case, assimilating data only from the surface layer has cascading effects throughout the water column. As discussed above, when the perfect synthetic data were assimilated, the true parameter values were recovered precisely and thus the subsurface fields were perfectly recovered as well. The more interesting results occurred when data with significant random noise were assimilated. Despite the presence of 40% noise in the synthetic data, the assimilation not only reduced the surface differences between the initial and true simulations of chlorophyll, POC, nitrate, and productivity, the assimilation also improved subsurface (depth-integrated) simulations of these variables by an equal or greater percentage (Table 6).

Together, these various methods for assessing the success of the twin experiments all demonstrate that the presence of significant random noise in the assimilated satellite data does not necessarily preclude the optimization from successfully identifying a reasonable approximation of the true simulation.

4.2. The Critical Importance of Assimilating Data at Multiple Sites

When data were assimilated individually at each of the sites, the resulting Assimilation Costs were low, both for the twin experiments (Table 4) and for the experiments assimilating actual satellite-derived data (Table 5). The fact that these individually optimized simulations fit the assimilated data better than the initial simulations and better than the simultaneously optimized simulations would appear to suggest that assimilating data individually at multiple sites produces more optimal results than assimilating data simultaneously at multiple sites. However, this is not the case. In fact, the individually optimized simulations fit the data better than the simulation used to derive the synthetic data (Individual Cost $<$ True Cost in Table 4), indicating that the optimization procedure was ultimately fitting the noise in the data. As a result, many of the normalized optimal parameter values from the individual experiments were highly unrealistic (Figures 6a and 9a). This overtuning of the optimized parameters did not occur, or at least was much less pronounced, when more data from multiple sites were available for assimilation. Thus, even though lower cost functions were obtained when assimilating data individually at each of the sites, more robust results were obtained when the model was required to fit data at multiple sites simultaneously.

Because the Individual twin experiments produced lower costs than the Simultaneous twin experiments (Table 4), one might expect that the RMSDs computed between the true simulation and the optimized simulations to be lower for the Individual experiments than for the Simultaneous experiments; again this was not the case. In fact, although the overtuning issue described above resulted in the optimized simulation matching the assimilated noisy data better when the model was tuned individually to each site, the overtuned parameters resulted in optimized simulations that did not successfully reproduce the true simulation at times and depths when data were not available: the RMSDs computed for the Individual Assimilation experiments were consistently higher than those computed for the Simultaneous Assimilation experiments (Table 6). In summary, assimilating synthetic data simultaneously from all four sites not only resulted in more realistic parameter values (Figure 6), but also generated an optimized solution that provided an improved fit, even at times and depths for which data were not assimilated, and even for variables that were not assimilated (Table 6).

Similar results were also obtained when assimilating actual satellite-derived data fields, however in these experiments the "true" simulation is not known and thus RMSDs cannot be computed in the same way as in

Table 7. Case 1 Cross Validation Costs Generated by Applying the Parameter Values Individually Optimized for One Site to All Four Sites

Individual Optimization Site	A Priori Cost for All 4 Sites	A Posteriori Cost for All 4 Sites
N1	15.1	17.3
N2	15.1	231.3
S1	15.1	10.3
S2	15.1	$> 10^3$

the twin experiments. In this case, the validity of the individually optimized simulations was assessed by means of rigorous cross validation experiments conducted by applying the parameter values individually optimized for one site to the other three sites (Table 7). Only one out of the four resulting total costs in these Case 1 cross validation experiments was lower than the a priori cost. For example, when applying the optimal parameter set derived from individually assimilating the N2 Case 1 data to the other three sites, the resulting total cost from the four sites increased by more than 15 times compared to the original a priori cost and was nearly 25 times larger than the cost resulting from the Simultaneous experiment (Tables 5 and 7). For the only case in which the total a posteriori cost was lower than the a priori cost (i.e., assimilation of S1 data, cost = 10.3, Table 7), the cost was still higher than that generated in the Simultaneous assimilation experiment (cost = 8.8, Table 5).

These cross validation experiments suggest that although assimilating data from one site alone can significantly improve model performance at that particular site, the improved fit is largely due to overtuning and fitting data noise, and thus results in a deterioration of model performance when the parameter values are applied at other times and/or locations. As in the twin experiments assimilating synthetic data, the issue with overtuned parameters vanishes when data are simultaneously assimilated from multiple sites: when data from all four sites were simultaneously assimilated, the resulting optimal parameter set was well constrained (Figure 6b) and the cost function was still not substantially higher than that obtained from the Individual Assimilation experiments (Table 5).

These results regarding the problems associated with the application of overtuned parameters due to an underconstrained system are consistent with results from previous studies. For example, *Ward et al.* [2010] assimilated data from two sites individually and simultaneously, and demonstrated high uncertainty in the optimal parameters when data were assimilated from only one site. In another study, *Friedrichs et al.* [2006] conducted two sets of assimilation experiments with multiple models of varying complexity: in the first experiment all model parameters were optimized (10–19) and in the second only a subset of uncorrelated parameters (2–6) was estimated, using the same data set in both cases. The results of their cross validations indicated that the assimilated data did not provide enough information to successfully constrain all model parameters, and as a result the overtuned parameters resulted in very low costs for the assimilated data, but very high costs when the model was applied to unassimilated data fields. In contrast, when only a subset of parameters was optimized, the model produced slightly higher costs for the assimilated data, but much lower costs for the unassimilated data fields. These results are analogous to the results shown here for the experiments assimilating data from individual sites (which produced low costs for the assimilated data and very high costs/RMSD for unassimilated data) and the experiments assimilating data simultaneously from multiple sites (which produced slightly higher costs for the assimilated data, but much lower costs/RMSD for the unassimilated data).

Although the Individual Assimilation experiments conducted here resulted in unrealistic overtuned parameter values, this is likely at least partially due to the fact that only remotely sensed data (chlorophyll and POC) were assimilated. For example, *Bagniewski et al.* [2011] have shown that many parameters can be constrained when more complete observational data sets, including subsurface nutrients and oxygen, are also assimilated. However, they did note that their lack of zooplankton observations still leads to large uncertainties in model parameters for grazing.

Ultimately, the success we found in simultaneously assimilating remotely sensed data from multiple sites and the failure of assimilating such data from individual sites illustrates a problem inherent to the assimilation of moored data from individual locations, and highlights the advantage of assimilating information from satellites, which routinely includes synoptic data from multiple locations.

4.3. The Relative Importance of Assimilating Different Types of Satellite-Derived Data

In order to determine the relative benefit of assimilating different types of satellite-derived data, various assimilation cases were run which assimilated combinations of size-fractionated chlorophyll, total

chlorophyll, and/or POC. When satellite-derived POC data were assimilated without the concomitant assimilation of chlorophyll data, the model-data misfit for chlorophyll dramatically increased at the southern sites. The model was only able to successfully reproduce the POC observations by producing unrealistic chlorophyll concentrations. On the contrary, the assimilation of chlorophyll (or size-fractionated chlorophyll) without the concomitant assimilation of POC data only generated a small increase in the POC model-data misfit. This is likely because chlorophyll provides a better constraint on the model, as there are multiple ways by which the model can produce a given POC concentration (using different proportions of small/large phytoplankton, zooplankton, and detritus) but a smaller number of ways in which the model can produce a given chlorophyll concentration (using different proportions of large and small phytoplankton). For example, an increase in the maximum zooplankton-grazing rate could cause an increase in zooplankton and a decrease in phytoplankton, resulting in a significant change in chlorophyll but no net change in POC. For these reasons, the assimilation of satellite-derived chlorophyll provides a better constraint on the model than does the assimilation of POC.

The relatively minor improvements in the modeled POC fields, as compared to those of the modeled chlorophyll fields are also due to the fact that the POC distributions are more sensitive to physical processes that were included but not optimized in the model, such as vertical advection and sinking. In particular, the surface POC cost increased by more than 90% when detrital sinking was turned off, whereas the surface chlorophyll cost changed by less than 1%. Because the POC distributions are controlled more by physics and less by biological processes as compared to the chlorophyll distributions, the adjustments of the biological parameters tend to improve the chlorophyll distributions more than the POC concentrations.

In terms of the relative benefits of assimilating size-fractionated chlorophyll and total chlorophyll, the results are less clear; however, the assimilation of size-fractionated chlorophyll resulted in a greater percent reduction in the a priori cost function and also produced a lower model-data misfit for both size-fractionated chlorophyll as well as total chlorophyll. Thus, it appears that when implementing assimilative models with more than one phytoplankton size class, the assimilation of size-fractionated chlorophyll does provide an advantage over the assimilation of total chlorophyll.

In general, the lowest model-data misfits were obtained when size-fractionated chlorophyll was assimilated together with POC. Although size-fractionated chlorophyll was simulated best when POC was not assimilated, this did result in an increase in misfit for POC. These results suggest that when possible size-fractionated satellite chlorophyll and POC should both be simultaneously assimilated in order to provide the best possible fit to a given satellite data set.

5. Summary and Conclusions

Experiments were conducted to examine the effects of assimilating three types of satellite-derived products (chlorophyll, size-fractionated chlorophyll, and particulate organic carbon) into a one-dimensional lower trophic level marine ecosystem model of the Mid-Atlantic Bight. Although these results were obtained for a continental shelf region, we feel that similar results would be obtained if the study were repeated at sites in the open ocean. Twin experiments illustrated that the assimilative framework can reasonably successfully recover a set of carefully selected, uncorrelated ecosystem parameters, even when the synthetic data are associated with substantial levels of random noise. In addition, these twin assimilation experiments improved both surface and subsurface distributions of not only assimilated variables, but also of unassimilated variables such as nutrient concentrations and productivity.

Both the twin experiments and experiments assimilating actual satellite-derived data demonstrated that the optimization procedure only generated robust parameter values when data were simultaneously assimilated from multiple sites. Assimilating satellite-derived surface data at individual sites produced low-cost functions, but did not adequately constrain the model. In this case, the optimization procedure overtuned the model simulation, and as a result generated unrealistic parameter values that produced large model-data misfits at times and locations when data were not assimilated. In contrast, when data were assimilated from multiple sites simultaneously, the model was successfully constrained and robust parameter values were generated.

When POC data were assimilated without chlorophyll, model-data misfit for chlorophyll was substantially increased. In contrast, when chlorophyll (either total or size-differentiated) data were assimilated without

POC, the model-data misfit for POC was only slightly degraded. These results suggest that satellite-derived chlorophyll distributions act as a significantly greater constraint to the model than do satellite-derived POC distributions. Although the results are less clear regarding the relative advantages of assimilating size-differentiated chlorophyll rather than total chlorophyll, optimal results were obtained when both size-differentiated chlorophyll and POC were both assimilated.

This data assimilative modeling study provides an example of how multiple satellite-derived products can be simultaneously used to optimize marine ecosystem models. The effects of assimilating the satellite data were apparent at depths well below the surface layer, however vertical profile data are required to further evaluate these changes. We expect that satellite-derived size-fractionated chlorophyll concentrations may play an increasingly important role in the future, as assimilative methods are applied to more complex ecosystem models that incorporate multiple phytoplankton and zooplankton compartments.

Appendix A: Model Equations

The model equations are included below for reference. State variables are defined as: DS, small detritus; DL, large detritus; NO_3, nitrate; NH_4, ammonium; PS, small phytoplankton; PL, large phytoplankton; Z, zooplankton; ChlS, small chlorophyll; ChlL, large chlorophyll. Model parameterizations are described more fully in *Fennel et al*. [2006] and parameter values, except for those specifically noted in Table 1, are identical to those used in *Fennel et al*. [2008].

A1. State Variable Equations

Change in Small P = Small P growth − Z grazing of Small P − mortality of Small P −aggregation of Small P − sinking of Small P

$$\frac{\partial PS}{\partial t}=\mu_{PS}PS-g_{PS\_Z}Z-m_PPS-\tau(DS+PS+PL)PS-w_{PS}\frac{\partial PS}{dz}$$

Change in Large P = Large P growth − Z grazing of Large P − mortality of Large P −aggregation of Large P − sinking of Large P

$$\frac{\partial PL}{\partial t}=\mu_{PL}PL-g_{PL\_Z}Z-m_PPL-\tau(DS+PS+PL)PL-w_{PS}\frac{\partial PL}{dz}$$

Change in Z = assimilation of grazed P − Z excretion to ammonium (linear term and assimilation-dependent term) − mortality of Z

$$\frac{\partial Z}{\partial t}=(g_{PS\_Z}+g_{PL\_Z})\beta Z-(I_{BM\_Z}+I_E\frac{(PS+PL)^2}{k_P+(PS+PL)^2}\beta)Z-m_ZZ^2$$

Change in Small Detritus = unassimilated Z grazing of Small and Large P + mortality of Z + mortality of Small P and Large P − aggregation of Small Detritus − remineralization of Small Detritus − sinking of Small Detritus

$$\frac{\partial DS}{\partial t}=(g_{PS\_Z}+g_{PL\_Z})(1-\beta)Z+m_ZZ^2+m_P(PS+PL)-\tau(DS+PS+PL)SD-r_{DS}DS-w_{DS}\frac{\partial DS}{\partial z}$$

Change in Large Detritus = aggregation of Small Detritus, Small P and Large P − remineralization of Large Detritus − sinking of Large Detritus

$$\frac{\partial DL}{\partial t}=\tau(DS+PS+LP)^2-r_{DL}DL-w_{DL}\frac{\partial DL}{\partial z}$$

Change in Nitrate = −Small P uptake of nitrate − Large P uptake of nitrate + nitrification

$$\frac{\partial NO3}{\partial t} = -\mu_{PS\_NO3} PS - \mu_{LP\_NO3} PL + nNH4$$

Change in Ammonium = −Small P uptake of ammonium − Large P uptake of ammonium − nitrification + Z excretion (linear term and assimilation-dependent term) + remineralization of Small Detritus + remineralization of Large Detritus

$$\frac{\partial NH4}{\partial t} = -\mu_{PS\_NH4} PS - \mu_{PL\_NH4} PL - nNH4 + (l_{BM\_Z} + l_E \frac{(PS+PL)^2}{k_P + (PS+PL)^2}\beta) Z + r_{DS} DS + r_{DL} DL$$

Change in Small Chlorophyll = Small P growth − Z grazing of Small P − mortality of Small P − aggregation of Small P − sinking of Small P − sinking of Small P

$$\frac{\partial ChlS}{\partial t} = \rho_{ChlS} \mu_{PS} ChlS - g_{PS\_Z} Z \frac{ChlS}{PS} - m_P ChlS - \tau(DS+PS+PL) ChlS - w_{PS} \frac{\partial ChlS}{dz}$$

Change in Large Chlorophyll = Large P growth − Z grazing of Large P − mortality of Large P − aggregation of Large P − sinking of Large P

$$\frac{\partial ChlL}{\partial t} = \rho_{ChlL} \mu_{PL} ChlL - g_{PL\_Z} Z \frac{ChlL}{PL} - m_P ChlL - \tau(DS+PS+PL) ChlL - w_{PL} \frac{\partial ChlL}{dz}$$

A2. Definitions of Functional Formulations Used in Above Equations

$$g_{PS\_Z} = g_{max_P S\_Z} \frac{PS^2}{k_P + PS^2}$$

$$\rho_{ChlS} = \frac{\theta_{max\_PS} \mu_{PS} \cdot PS}{\alpha I \cdot ChlS}$$

$$f_{PS}(I) = \frac{\alpha I}{\sqrt{\mu_{max\_PS}^2 + \alpha^2 I^2}}$$

$$L_{NO3\_PS} = \left(\frac{NO3}{k_{NO3\_PS} + NO3}\right)\left(1 + \frac{NH4}{k_{NH4}}\right)^{-1}$$

$$L_{NH4} = \frac{NH4}{k_{NH4} + NH4}$$

$$\mu_{PS} = \mu_{max\_PS} f_{PS}(I)(L_{NO3\_SP} + L_{NH4})$$

$$\mu_{PS\_NO3} = \mu_{max\_PS} f_{PS}(I) L_{NO3\_PS}$$

$$\mu_{PS\_NH4} = \mu_{max\_PS} f_{PS}(I) L_{NH4}$$

$$g_{PL\_Z} = g_{max\_PL\_Z} \frac{PL^2}{k_P + PL^2}$$

$$\rho_{ChlL} = \frac{\theta_{max\_PL} \mu_{PL} \cdot PL}{\alpha I \cdot ChlL}$$

$$f_{PL}(I) = \frac{\alpha I}{\sqrt{\mu_{max\_PL}^2 + \alpha^2 I^2}}$$

$$L_{NO3\_PL} = \left(\frac{NO3}{k_{NO3\_PL} + NO3}\right)\left(1 + \frac{NH4}{k_{NH4}}\right)^{-1}$$

$$\mu_{PL} = \mu_{max\_PL} f_{PL}(I)(L_{NO3\_PL} + L_{NH4})$$

$$\mu_{PL\_NO3} = \mu_{max\_PL} f_{PL}(I) L_{NO3\_PL}$$

$$\mu_{PL\_NH4} = \mu_{max\_PL} f_{PL}(I) L_{NH4}$$

Acknowledgments
This work was supported by NASA Headquarters under the NASA Earth and Space Science Fellowship Program (NNX10AN50H) and the Interdisciplinary Science Program (NNX11AD47G). Computer facilities and support were provided by the High Performance Clusters Pacific at Virginia Institute of Marine Science, College of William and Mary. The authors would like to thank the NASA U.S. Eastern Continental Shelf Carbon Cycling (USECoS) group for their useful comments. In particular, we are grateful to Kimberly Hyde, Xiaoju Pan, and Antonio Mannino for providing the satellite-derived size-fractionated chlorophyll data. The authors would like to thank the SeaWiFS Project (Code 970.2) and the Distributed Active Archive Center (Code 610.2) at the Goddard Space Flight Center, Greenbelt, MD 20771, for the production and distribution of these data, respectively. This is VIMS contribution 3357.

References

Alvain, S., C. Moulin, Y. Dandonneau, and F. M. Breon (2005), Remote sensing of phytoplankton groups in case 1 waters from global SeaWiFS imagery, *Deep Sea Res., Part I*, *52*(11), 1989–2004, doi:10.1016/j.dsr.2005.06.015.

Armstrong, R. A. (1999), Stable model structures for representing biogeochemical diversity and size spectra in plankton communities, *J. Plankton Res.*, *21*(3), 445–464, doi:10.1093/plankt/21.3.445.

Aumont, O., E. Maier-Reimer, S. Blain, and P. Monfray (2003), An ecosystem model of the global ocean including Fe, Si, P colimitations, *Global Biogeochem. Cycles*, *17*(2), 1060, doi:10.1029/2001GB001745.

Bagniewski, W., K. Fennel, M.J. Perry, and E. A. D'Asaro (2011), Optimizing models of the North Atlantic spring bloom using physical, chemical and bio-optical observations from a Lagrangian float, *Biogeosciences*, *8*, 1291–1307, doi:10.5194/bg-8-1291-2011.

Brewin, R. J. W., S. Sathyendranath, T. Hirata, S. J. Lavender, R. M. Barciela, and N. J. Hardman-Mountford (2010), A three-component model of phytoplankton size class for the Atlantic Ocean, *Ecol. Modell.*, *221*(11), 1472–1483, doi:10.1016/j.ecolmodel.2010.02.014.

Carder, K. L., F. R. Chen, Z. P. Lee, and S. K. Hawes (1999), Semianalytic moderate-resolution imaging spectrometer algorithms for chlorophyll a and absorption with bio-optical domains based on nitrate-depletion temperatures, *J. Geophys. Res.*, *104*, 5403–5421.

Chai, F., M. S. Jiang, Y. Chao, R. C. Dugdale, F. Chavez, and R. T. Barber (2007), Modeling responses of diatom productivity and biogenic silica export to iron enrichment in the equatorial Pacific Ocean, *Global Biogeochem. Cycles*, *21*, GB3S90, doi:10.1029/2006GB002804.

Crispi, G., M. Pacciaroni, and D. Viezzoli (2006), Simulating biomass assimilation in a Mediterranean ecosystem model using SOFA: Setup and identical twin experiments, *Ocean Sci.*, *2*(2), 123–136.

Cullen, J. T., Z. Chase, K. H. Coale, S. E. Fitzwater, and R. M. Sherrell (2003), Effect of iron limitation on the cadmium to phosphorus ratio of natural phytoplankton assemblages from the Southern Ocean, *Limnol. Oceanogr.*, *48*(3), 1079–1087.

Druon, J. N., A. Mannino, S. Signorini, C. McClain, M. Friedrichs, J. Wilkin, and K. Fennel (2010), Modeling the dynamics and export of dissolved organic matter in the Northeastern U.S. continental shelf, *Estuarine Coastal Shelf Sci.*, *88*(4), 488–507.

Dugdale, R., F. Chai, R. Feely, C. Measures, A. Parker, and F. Wilkerson (2011), The regulation of equatorial Pacific new production and pCO_2 by silicate-limited diatoms, *Deep Sea Res., Part II*, *58*(3–4), 477–492, doi:10.1016/j.dsr2.2010.08.008.

Eckhardt, K., and J. G. Arnold (2001), Automatic calibration of a distributed catchment model, *J. Hydrol.*, *251*(1–2), 103–109, doi:10.1016/s0022-1694(01)00429-2.

Fan, W., and X. Lv (2009), Data assimilation in a simple marine ecosystem model based on spatial biological parameterizations, *Ecol. Modell.*, *220*(17), 1997–2008, doi:10.1016/j.ecolmodel.2009.04.050.

Fasham, M. J. R., H. W. Ducklow, and S. M. McKelvie (1990), A nitrogen-based model of plankton dynamics in the oceanic mixed layer, *J. Mar. Res.*, *48*(3), 591–639.

Fasham, M. J. R., J. L. Sarmiento, R. D. Slater, H. W. Ducklow, and R. Williams (1993), Ecosystem behavior at Bermuda Station "S" and ocean weather station "India": A general circulation model and observational analysis, *Global Biogeochem. Cycles*, *7*(2), 379–415, doi:10.1029/92gb02784.

Fennel, K., M. Losch, J. Schröter, and M. Wenzel (2001), Testing a marine ecosystem model: Sensitivity analysis and parameter optimization, *J. Mar. Syst.*, *28*(1–2), 45–63, doi:10.1016/s0924-7963(00)00083-x.

Fennel, K., J. Wilkin, J. Levin, J. Moisan, J. O'Reilly, and D. Haidvogel (2006), Nitrogen cycling in the Middle Atlantic Bight: Results from a three-dimensional model and implications for the North Atlantic nitrogen budget, *Global Biogeochem. Cycles*, *20*, GB3007, doi:10.1029/2005GB002456.

Fennel, K., J. Wilkin, M. Previdi, and R. Najjar (2008), Denitrification effects on air-sea CO_2 flux in the coastal ocean: Simulations for the northwest North Atlantic, *Geophys. Res. Lett.*, *35*, L24608, doi:10.1029/2008GL036147.

Fennel, K., R. Hetland, Y. Feng, and S. DiMarco (2011), A coupled physical-biological model of the Northern Gulf of Mexico shelf: Model description, validation and analysis of phytoplankton variability, *Biogeosciences*, *8*(7), 1881–1899, doi:10.5194/bg-8-1881-2011.

Fitzpatrick, J. J. (2009), Assessing skill of estuarine and coastal eutrophication models for water quality managers, *J. Mar. Syst.*, *76*(1–2), 195–211, doi:10.1016/j.jmarsys.2008.05.018.

Fontana, C., C. Grenz, C. Pinazo, P. Marsaleix, and F. Diaz (2009), Assimilation of SeaWiFS chlorophyll data into a 3D-coupled physical-biogeochemical model applied to a freshwater-influenced coastal zone, *Cont. Shelf Res.*, *29*(11–12), 1397–1409, doi:10.1016/j.csr.2009.03.005.

Friedrichs, M. A. M. (2001), A data assimilative marine ecosystem model of the central equatorial Pacific: Numerical twin experiments, *J. Mar. Res.*, *59*(6), 859–894, doi:10.1357/00222400160497544.

Friedrichs, M. A. M. (2002), Assimilation of SeaWiFS and JGOFS EqPac data into a marine ecosystem model of the central equatorial Pacific, *Deep Sea Res., Part II*, *49*, 289–319.

Friedrichs, M. A. M., and E. E. Hofmann (2001), Physical control of biological processes in the central equatorial Pacific Ocean, *Deep Sea Res., Part I*, *48*, 1023–1069, doi:10.1016/S0967-0637(00)00079-0.

Friedrichs, M. A. M., R. Hood, and J. Wiggert (2006), Ecosystem model complexity versus physical forcing: Quantification of their relative impact with assimilated Arabian Sea data, *Deep Sea Res., Part II*, *53*, 576–600.

Friedrichs, M. A. M., et al. (2007), Assessment of skill and portability in regional marine biogeochemical models: Role of multiple phytoplankton groups, *J. Geophys. Res.*, *112*, C08001, doi:10.1029/2006JC003852.

Friedrichs, M. A. M., et al. (2009), Assessing the uncertainties of model estimates of primary productivity in the tropical Pacific Ocean, *J. Mar. Syst.*, *76*(1–2), 113–133, doi:10.1016/j.jmarsys.2008.05.010.

Fujii, M., Y. Yamanaka, Y. Nojiri, M. J. Kishi, and F. Chai (2007), Comparison of seasonal characteristics in biogeochemistry among the subarctic North Pacific stations described with a NEMURO-based marine ecosystem model, *Ecol. Modell.*, *202*(1–2), 52–67, doi:10.1016/j.ecolmodel.2006.02.046.

Gan, J., Z. Lu, M. Dai, A. Y. Y. Cheung, H. Liu, and P. Harrison (2010), Biological response to intensified upwelling and to a river plume in the northeastern South China Sea: A modeling study, *J. Geophys. Res.*, *115*, C09001, doi:10.1029/2009JC005569.

Garcia-Gorriz, E., N. Hoepffner, and M. Ouberdous (2003), Assimilation of SeaWiFS data in a coupled physical-biological model of the Adriatic Sea, *J. Mar. Syst.*, *40*, 233–252, doi:10.1016/s0924-7963(03)00020-4.

Gege, P. (1998), Characterization of the phytoplankton in Lake Constance for classification by remote sensing, *Arch. Hydrobiol.*, *53*, 179–193.

Geider, R. J., H. L. MacIntyre, and T. M. Kana (1997), Dynamic model of phytoplankton growth and acclimation: Responses of the balanced growth rate and the chlorophyll a:carbon ratio to light, nutrient-limitation and temperature, *Mar. Ecol. Prog. Ser.*, *148*, 187–200.

Giering, R., and T. Kaminski (1998), Recipes for adjoint code construction, *ACM Trans. Math. Software*, *24*(4), 437–474, doi:10.1145/293686.293695.

Gilbert, J. C., and C. Lemaréchal (1989), Some numerical experiments with variable-storage quasi-Newton algorithms, *Math. Program.*, *45*(1), 407–435, doi:10.1007/bf01589113.
Gregg, W. W., M. A. M. Friedrichs, A. R. Robinson, K. A. Rose, R. Schlitzer, K. R. Thompson, and S. C. Doney (2009), Skill assessment in ocean biological data assimilation, *J. Mar. Syst.*, *76*(1–2), 16–33, doi:10.1016/j.jmarsys.2008.05.006.
Hemmings, J. C. P., and P. G. Challenor (2012), Addressing the impact of environmental uncertainty in plankton model calibration with a dedicated software system: The Marine Model Optimization Testbed (MarMOT 1.1 alpha), *Geosci. Model Dev.*, *5*(2), 471–498, doi:10.5194/gmd-5-471-2012.
Hemmings, J. C. P., M. A. Srokosz, P. Challenor, and M. J. R. Fasham, (2004), Split-domain calibration of an ecosystem model using satellite ocean colour data, *J. Mar. Syst.*, *50* (3–4). 141–179, 10.1016/j.jmarsys.2004.02.003.
Hirata, T., et al. (2011), Synoptic relationships between surface Chlorophyll-a and diagnostic pigments specific to phytoplankton functional types, *Biogeosciences*, *8*(2), 311–327, doi:10.5194/bg-8-311-2011.
Hofmann, E., et al. (2008), Eastern US continental shelf carbon budget integrating models, data assimilation, and analysis, *Oceanography*, *21*(1), 86–104.
Hofmann, E. E., and M. A. M. Friedrichs (2001), Biogeochemical data assimilation, in *Encyclopedia of Ocean Sciences*, edited by J. H. Steele et al., pp. 302–308, Academic, London.
Hofmann, E. E., et al. (2011), Modeling the dynamics of continental shelf carbon, *Annu. Rev. Mar. Sci.*, 93–122, doi:10.1146/Annurev-Marine-120709-142740.
Hoge, F. E., and P. E. Lyon (2002), Satellite observation of chromophoric dissolved organic matter (CDOM) variability in the wake of hurricanes and typhoons, *Geophys. Res. Lett.*, *29*(19), 1908, doi:10.1029/2002GL015114.
Hood, R. R., N. R. Bates, D. G. Capone, and D. B. Olson (2001), Modeling the effect of nitrogen fixation on carbon and nitrogen fluxes at BATS, *Deep Sea Res., Part II*, *48*(8–9), 1609–1648.
Hood, R. R., et al. (2006), Pelagic functional group modeling: Progress, challenges and prospects, *Deep Sea Res., Part II*, *53*(5–7), 459–512, doi:10.1016/j.dsr2.2006.01.025.
Hovis, W. A., et al. (1980), Nimbus-7 coastal zone color scanner: System description and initial imagery, *Science*, *210*(4465), 60–63, doi:10.1126/science.210.4465.60.
Hu, J., K. Fennel, J. P. Mattern, and J. Wilkin (2012), Data assimilation with a local Ensemble Kalman Filter applied to a three-dimensional biological model of the Middle Atlantic Bight, *J. Mar. Syst.*, *94*(0), 145–156, doi:10.1016/j.jmarsys.2011.11.016.
Hundsdorfer, W., and R. A. Trompert (1994), Method of lines and direct discretization: A comparison for linear advection, *Appl. Numer. Math.*, *13*(6), 469–490, doi:10.1016/0168-9274(94)90009-4.
Kidston, M., R. Matear, and M. E. Baird (2011), Parameter optimisation of a marine ecosystem model at two contrasting stations in the Sub-Antarctic Zone, *Deep Sea Res. Part II*, *58*(21–22), 2301–2315, doi:10.1016/j.dsr2.2011.05.018.
Kishi, M. J., et al. (2007), NEMURO—A lower trophic level model for the North Pacific marine ecosystem, *Ecol. Modell.*, *202*, 12–25, 10.1016/j.ecolmodel.2006.08.021.
Kuroda, H., and M. J. Kishi (2004), A data assimilation technique applied to estimate parameters for the NEMURO marine ecosystem model, *Ecol. Modell.*, *172*(1), 69–85, doi:10.1016/j.ecolmodel.2003.08.015.
Lawson, L. M., Y. H. Spitz, E. E. Hofmann, and R. B. Long (1995), A data assimilation technique applied to a predator-prey model, *Bull. Math. Biol.*, *57*(4), 593–617, doi:10.1016/S0092–8240(05)80759-1.
Lawson, L. M., E. E. Hofmann, and Y. H. Spitz (1996), Time series sampling and data assimilation in a simple marine ecosystem model, *Deep Sea Res., Part II*, *43*(2–3), 625–651, doi:10.1016/0967-0645(95)00096-8.
Le Quere, C., et al. (2005), Ecosystem dynamics based on plankton functional types for global ocean biogeochemistry models, *Global Change Biol.*, *11*(11), 2016–2040, doi:10.1111/j.1365-2468.2005.01004.x.
Leredde, Y., C. Lauer-Leredde, and F. Diaz (2005), On the variational data assimilation by a marine ecosystem model of NPZ type, *Comptes Rendus Geosci.*, *337*(12), 1055–1064, doi:10.1016/j.crte.2005.05.003.
Lima, I. D., D. B. Olson, and S. C. Doney (2002), Intrinsic dynamics and stability properties of size-structured pelagic ecosystem models, *J. Plankton Res.*, *24*(6), 533–556.
Lomas, M. W., and S. B. Moran (2011), Evidence for aggregation and export of cyanobacteria and nano-eukaryotes from the Sargasso Sea euphotic zone, *Biogeosciences*, *8*(1), 203–216, doi:10.5194/bg-8-203-2011.
Luo, Y. W., M. A. M. Friedrichs, S. C. Doney, M. J. Church, and H. W. Ducklow (2010), Oceanic heterotrophic bacterial nutrition by semilabile DOM as revealed by data assimilative modeling, *Aquat. Microbial Ecol.*, *60*(3), 273–287, doi:10.3354/ame01427.
Luo, Y. W., H. W. Ducklow, M. A. M. Friedrichs, M. J. Church, D. M. Karl, and S. C. Doney (2012), Interannual variability of primary production and dissolved organic nitrogen storage in the North Pacific Subtropical Gyre, *J. Geophys. Res.*, *117*, G03019, doi:10.1029/2011JG001830.
Marra, J., C. C. Trees, and J. E. O'Reilly (2007), Phytoplankton pigment absorption: A strong predictor of primary productivity in the surface ocean, *Deep Sea Res., Part I*, *54*(2), 155–163, doi:10.1016/j.dsr.2006.12.001.
Matear, R. J. (1995), Parameter optimization and analysis of ecosystem models using simulated annealing: A case study at Station P, *J. Mar. Res.*, *53*(4), 571–607, doi:10.1357/0022240953213098.
Mattern, J. P., M. Dowd, and K. Fennel (2010), Sequential data assimilation applied to a physical-biological model for the Bermuda Atlantic time series station, *J. Mar. Syst.*, *79*(1–2), 144–156, doi:10.1016/j.jmarsys.2009.08.004.
Mattern, J. P., K. Fennel, and M. Dowd (2012), Estimating time-dependent parameters for a biological ocean model using an emulator approach, *J. Mar. Syst.*, *96–97*, 32–47, doi:10.1016/j.jmarsys.2012.01.015.
Mattern, J. P., M. Dowd, and K. Fennel (2013), Particle filter-based data assimilation for a three-dimensional biological ocean model and satellite observations, *J. Geophys. Res.*, *118*, 2746–2760, doi:10.1002/jgrc.20213.
Mauriac, R., T. Moutin, and M. Baklouti (2011), Accumulation of DOC in Low Phosphate Low Chlorophyll (LPLC) area: Is it related to higher production under high N:P ratio?, *Biogeosciences*, *8*(4), 933–950, doi:10.5194/bg-8-933-2011.
McClain, C. R. (2009), A decade of satellite ocean color observations, *Annu. Rev. Mar. Sci.*, *1*, 19–42, doi:10.1146/annurev.marine.010908.163650.
McDonald, C. P., V. Bennington, N. R. Urban, and G. A. McKinley (2012), 1-D test-bed calibration of a 3-D Lake Superior biogeochemical model, *Ecol. Modell.*, *225*, 115–126, doi:10.1016/j.ecolmodel.2011.11.021.
McGillicuddy, D. J., D. R. Lynch, A. M. Moore, W. C. Gentleman, C. S. Davis, and C. J. Meise (1998), An adjoint data assimilation approach to diagnosis of physical and biological controls on *Pseudocalanus* spp. in the Gulf of Maine-Georges Bank region, *Fish. Oceanogr.*, *7*, 205–218.
Mishnov, A. V., W. D. Gardner, and R. M. J. (2003), Remote sensing and surface POC concentration in the South Atlantic, *Deep Sea Res., Part II*, *50*, 2997–3015.

Moore, J. K., S. C. Doney, J. A. Kleypas, D. M. Glover, and I. Y. Fung (2002), An intermediate complexity marine ecosystem model for the global domain, *Deep Sea Res., Part II*, *49*(1–3), 403–462, doi:10.1016/s0967-0645(01)00108-4.
Morel, A., and B. Gentili (2009), A simple band ratio technique to quantify the colored dissolved and detrital organic material from ocean color remotely sensed data, *Remote Sens. Environ.*, *113*(5), 998–1011, doi:10.1016/j.rse.2009.01.008.
Mouw, C. B., and J. A. Yoder (2005), Primary production calculations in the Mid-Atlantic Bight, including effects of phytoplankton community size structure, *Limnol. Oceanogr.*, *50*(4), 1232–1243.
Nair, A., S. Sathyendranath, T. Platt, J. Morales, V. Stuart, M. H. Forget, E. Devred, and H. Bouman (2008), Remote sensing of phytoplankton functional types, *Remote Sens. Environ.*, *112*(8), 3366–3375, doi:10.1016/j.rse.2008.01.021.
Natvik, L. J., and G. Evensen (2003), Assimilation of ocean colour data into a biochemical model of the North Atlantic: Part 1. Data assimilation experiments, *J. Mar. Syst.*, *40–41*, 127–153, doi:10.1016/S0924-7963(03)00016-20.
O'Reilly, J. E., S. Maritorena, B. G. Mitchell, D. A. Siegel, K. L. Carder, S. A. Garver, M. Kahru, and C. McClain (1998), Ocean color chlorophyll algorithms for SeaWiFS, *J. Geophys. Res.*, *103*(C11), 24,937–24,953, doi:10.1029/98JC02160.
O'Reilly, J. E., et al. (2000), SeaWiFS postlaunch calibration and validation analyses, Part 3, in *SeaWiFS Postlaunch Technical Report Series*, edited by S. B. Hooker and R. R. Firestone, NASA, Greenbelt, Md.
Oreskes, N., K. Shrader-Frechette, and K. Belitz (1994), Verification, validation, and confirmation of numerical models in the earth sciences, *Science*, *263*(5147), 641–646, doi:10.1126/science.263.5147.641.
Pan, X., A. Mannino, M. E. Russ, S. B. Hooker, and L. W. Harding Jr. (2010), Remote sensing of phytoplankton pigment distribution in the United States northeast coast, *Remote Sens. Environ.*, *114*(11), 2403–2416, doi:10.1016/j.rse.2010.05.015.
Pan, X., A. Mannino, H. G. Marshall, K. C. Filippino, and M. R. Mulholland (2011), Remote sensing of phytoplankton community composition along the northeast coast of the United States, *Remote Sens. Environ.*, *115*(12), 3731–3747, doi:10.1016/j.rse.2011.09.011.
Pelc, J. S., E. Simon, L. Bertino, G. El Serafy, and A. W. Heemink (2012), Application of model reduced 4D-Var to a 1D ecosystem model, *Ocean Modell.*, *57–58*, 43–58, doi:10.1016/j.ocemod.2012.09.003.
Pinker, R. T., M. Zhao, H. Wang, and E. F. Wood (2010), Impact of satellite based PAR on estimates of terrestrial net primary productivity, *Int. J. Remote Sens.*, *31*(19), 5221–5237, doi:10.1080/01431161.2010.496474.
Prieß, M., J. Piwonski, S. Koziel, A. Oschlies, and T. Slawig (2013), Accelerated parameter identification in a 3D marine biogeochemical model using surrogate-based optimization, *Ocean Modell.*, *68*, 22–36, doi:10.1016/j.ocemod.2013.04.003.
Rose, K. A., R. B. Cook, A. L. Brenkert, R. H. Gardner, and J. P. Hettelingh (1991), Systematic comparison of ILWAS, MAGIC, and ETD watershed acidification models: 1. Mapping among model inputs and deterministic results, *Water Resour. Res.*, *27*(10), 2577–2589, doi:10.1029/91WR01718.
Rose, K. A., B. A. Megrey, F. E. Werner, and D. M. Ware (2007), Calibration of the NEMURO nutrient-phytoplankton-zooplankton food web model to a coastal ecosystem: Evaluation of an automated calibration approach, *Ecol. Modell.*, *202*(1–2), 38–51, doi:10.1016/j.ecolmodel.2006.08.016.
Ryan, J.P., J.A. Yoder, and P.C. Cornillon (1999), Enhanced chlorophyll at the shelfbreak of the Mid-Atlantic Bight and Georges Bank during the spring transition, *Limnol. Oceanogr.*, *44*(1), 1–11.
Saba, V. S., et al. (2011), An evaluation of ocean color model estimates of marine primary productivity in coastal and pelagic regions across the globe, *Biogeosciences*, *8*(2), 489–503, doi:10.5194/bg-8-489-2011.
Schartau, M., A. Oschlies, and J. Willebrand (2001), Parameter estimates of a zero-dimensional ecosystem model applying the adjoint method, *Deep Sea Res., Part II*, *48*(8–9), 1769–1800, doi:10.1016/s0967-0645(00)00161-2.
Shchepetkin, A. F., and J. C. McWilliams (2005), The regional oceanic modeling system (ROMS): A split-explicit, free-surface, topography-following-coordinate oceanic model, *Ocean Modell.*, *9*, 347–404.
Spitz, Y. H., J. R. Moisan, M. R. Abbott, and J. G. Richman (1998), Data assimilation and a pelagic ecosystem model: Parameterization using time series observations, *J. Mar. Syst.*, *16*(1–2), 51–68, doi:10.1016/s0924–7963(97)00099-7.
Stemmann, L., G. A. Jackson, and D. Ianson (2004), A vertical model of particle size distributions and fluxes in the midwater column that includes biological and physical processes—Part I: Model formulation, *Deep Sea Res., Part I*, *51*(7), 865–884, doi:10.1016/j.dsr.2004.03.001.
Stow, C. A., J. Jolliff, D. J. McGillicuddy Jr., S. C. Doney, J. I. Allen, M. A. M. Friedrichs, K. A. Rose, and P. Wallhead (2009), Skill assessment for coupled biological/physical models of marine systems, *J. Mar. Syst.*, *76*(1–2), 4–15, doi:10.1016/j.jmarsys.2008.03.011.
Stramska, M., and D. Stramski (2005), Variability of particulate organic carbon concentration in the north polar Atlantic based on ocean color observations with sea-viewing wide field-of-view sensor (SeaWiFS), *J. Geophys. Res.*, *110*, C10018, doi:10.1029/2004JC002762.
Stramski, D., et al. (2008), Relationships between the surface concentration of particulate organic carbon and optical properties in the eastern South Pacific and eastern Atlantic Oceans, *Biogeosciences*, *5*(1), 171–201, doi:10.5194/bg-5–171-2008.
Sweby, P. (1984), High resolution schemes using flux limiters for hyperbolic conservation laws, *SIAM J. Numer. Anal.*, *21*(5), 995–1011, doi:10.1137/0721062.
Thacker, W. C. (1989), The role of the Hessian Matrix in fitting models to measurements, *J. Geophys. Res.*, *94*(C5), 6177–6196, doi:10.1029/JC094iC05p06177.
Tjiputra, J. F., D. Polzin, and A. M. E. Winguth (2007), Assimilation of seasonal chlorophyll and nutrient data into an adjoint three-dimensional ocean carbon cycle model: Sensitivity analysis and ecosystem parameter optimization, *Global Biogeochem. Cycles*, *21*, GB1001, doi:10.1029/2006GB002745.
Uitz, J., H. Claustre, A. Morel, and S. B. Hooker (2006), Vertical distribution of phytoplankton communities in open ocean: An assessment based on surface chlorophyll, *J. Geophys. Res.*, *111*, C08005, doi:10.1029/2005jc003207.
Vidussi, F., H. Claustre, B. B. Manca, A. Luchetta, and J. C. Marty (2001), Phytoplankton pigment distribution in relation to upper thermocline circulation in the eastern Mediterranean Sea during winter, *J. Geophys. Res.*, *106*(C9), 19,939–19,956, doi:10.1029/1999jc000308.
Vrugt, J. A., H. V. Gupta, W. Bouten, and S. Sorooshian (2003), A Shuffled Complex Evolution Metropolis algorithm for optimization and uncertainty assessment of hydrologic model parameters, *Water Resour. Res.*, *39*(8), 1201, doi:10.1029/2002WR001642.
Ward, B. A., M. A. M. Friedrichs, T. R. Anderson, and A. Oschlies (2010), Parameter optimisation techniques and the problem of underdetermination in marine biogeochemical models, *J. Mar. Syst.*, *81*, 34–43, doi:10.1016/j.jmarsys.2009.12.005.
Xiao, Y., and M. A. M. Friedrichs (2014), Using biogeochemical data assimilation to assess the relative skill of multiple ecosystem models: Effects of increasing the complexity of the planktonic food web, *Biogeosci. Discuss.*, *11*, 481–520, doi:10.5194/bgd-11–481-2014.
Xing, X. G., A. Morel, H. Claustre, F. D'Ortenzio, and A. Poteau (2012), Combined processing and mutual interpretation of radiometry and fluorometry from autonomous profiling Bio-Argo floats: 2. Colored dissolved organic matter absorption retrieval, *J. Geophys. Res.*, *117*, C04022, doi:10.1029/2011jc007632.

Xu, Q., H. Lin, Y. G. Liu, X. Q. Lv, and Y. C. Cheng (2008), Data assimilation in a coupled physical-biological model for the Bohai Sea and the Northern Yellow Sea, *Mar. Freshwater Res.*, *59*(6), 529–539, doi:10.1071/mf07144.

Xue, Z., R. He, K. Fennel, W. J. Cai, S. Lohrenz, and C. Hopkinson (2013), Modeling ocean circulation and biogeochemical variability in the Gulf of Mexico, *Biogeosciences*, *10*, 7219–7234, doi:10.5194/bgd-10-7785-2013.

Yoder, J. A., W. E. Esaias, G. C. Feldman, and C. R. McClain (1988), Satellite Ocean Color—Status Report, *Oceanography*, *1*(1), 18–20.

Yoder, J. A., S. E. Schollaert, and J. E. O'Reilly (2002), Climatological phytoplankton chlorophyll and sea surface temperature patterns in continental shelf and slope waters off the northeast U.S. coast, *Limnol. Oceanogr.*, *47*(3), 672–682.